Quaternary Geochronology 14 (2012) 81–93

Contents lists available at SciVerse ScienceDirect

Quaternary Geochronology

journal homepage: www.elsevier.com/locate/quageo

Research paper

Hydrological control of the dead carbon fraction in a Holocene tropical speleothem

M.L. Griffiths [a,*], J. Fohlmeister [b], R.N. Drysdale [c], Q. Hua [d], K.R. Johnson [a], J.C. Hellstrom [e], M.K. Gagan [f], J.-x. Zhao [g]

[a] Department of Earth System Science, University of California, Irvine, CA 92697-3100, USA
[b] Heidelberg Academy of Sciences, c/o Institute for Environmental Physics, INF 229, 69120 Heidelberg, Germany
[c] School of Land and Environment, The University of Melbourne, Parkville, VIC 2010, Australia
[d] Australian Nuclear Science and Technology Organisation (ANSTO), Locked Bag 2001, Kirrawee DC NSW 2232, Australia
[e] School of Earth Sciences, The University of Melbourne, Parkville, Victoria 2010, Australia
[f] Research School of Earth Sciences, The Australian National University, Canberra, ACT 0200, Australia
[g] Centre for Microscopy and Microanalysis, The University of Queensland, Brisbane, QLD 4072, Australia

ARTICLE INFO

Article history:
Received 11 October 2011
Received in revised form
26 March 2012
Accepted 1 April 2012
Available online 12 April 2012

Keywords:
Radiocarbon
Dead carbon fraction
Speleothem
Indonesia
U-Th dating
Holocene

ABSTRACT

Over the past decade, a number of speleothem studies have used radiocarbon (^{14}C) to address a range of palaeoclimate problems. These have included the use of the bomb pulse ^{14}C to anchor chronologies over the last 60 years, the combination of U-Th and ^{14}C measurements to improve the radiocarbon age-calibration curve, and linking atmospheric ^{14}C variations with climate change. An issue with a number of these studies is how to constrain, or interpret, variations in the amount of radioactively dead carbon (i.e. the dead carbon fraction, or DCF) that reduces radiocarbon concentrations in speleothems. In this study, we use ^{14}C, stable-isotopes, and trace-elements in a U-Th dated speleothem from Flores, Indonesia, to examine DCF variations and their relationship with above-cave climate over the late Holocene and modern era. A strong association between the DCF and hydrologically-controlled proxy data suggests that more dead carbon was being delivered to the speleothem during periods of higher cave recharge (i.e. lower $\delta^{18}O$, $\delta^{13}C$ and Mg/Ca values), and hence stronger summer monsoon. To explore this relationship, we used a geochemical soil-karst model coupled with ^{14}C measurements through the bomb pulse to disentangle the dominant components governing DCF variability in the speleothem. We find that the DCF is primarily controlled by limestone dissolution associated with changes in open- versus closed-system conditions, rather than kinetic fractionation and/or variations in the age spectrum of soil organic matter above the cave. Therefore, we infer that periods of higher rainfall resulted in a higher DCF because the system was in a more closed state, which inhibited carbon isotope exchange between the karst water dissolved inorganic carbon and soil-gas CO_2, and ultimately led to a greater contribution of dead carbon from the bedrock.

Published by Elsevier B.V.

1. Introduction and background

Cave carbonates, or speleothems, are rapidly becoming one of the most important and versatile palaeoclimate archives available to Quaternary researchers (e.g., Wang et al., 2008; Drysdale et al., 2009; Dorale et al., 2010; Hoffmann et al., 2010). Consequently, a highly productive and growing speleothem community has emerged, which in the last five years has resulted in a proliferation of new techniques and applications (e.g. Kluge et al., 2008; Blyth et al., 2011), substantial refinements to existing technologies (Vonhof et al., 2006; Woodhead et al., 2006; Dublyansky and Spötl, 2009), and a renewed interest in geochemical and physical modelling of speleothem-forming processes (Scholz et al., 2009; Wackerbarth et al., 2010; Dreybrodt and Scholz, 2011; Fohlmeister et al., 2011b).

Some of the earliest speleothem research employed ^{14}C as a dating tool (Broecker et al., 1960; Hendy and Wilson, 1968), but up until recently it has played a very minor role in speleothem research because of the 'dead carbon' problem. This problem stems from the inclusion of bedrock-derived, 'radioactively dead' carbon into the total dissolved inorganic carbon (DIC) pool that is subsequently encoded into a growing speleothem. The result is an

* Corresponding author. Tel.: +1 949 444 4965; fax: +1 949 824 3874.
E-mail address: m.griffiths@uci.edu (M.L. Griffiths).

1871-1014/$ – see front matter Published by Elsevier B.V.
doi:10.1016/j.quageo.2012.04.001

'apparent' radiocarbon age for the speleothem that may differ significantly from the true radiocarbon age and thus cannot be converted to an age in 'cal yr BP' using the atmospheric ^{14}C calibration curve. The key concern is that the proportion of radioactively dead carbon at the time of deposition (expressed as the % dead carbon fraction, or DCF) varies from cave to cave (Genty et al., 2001; Oster et al., 2010; Hodge et al., 2011) according to site conditions (e.g. climate, overlying vegetation, karst architecture). Moreover, DCF may fluctuate according to local changes in soil-water-rock interaction (Genty and Massault, 1999; Genty et al., 2001) and variations in the age spectrum of soil organic matter (SOM) above the cave (Oster et al., 2010; Fohlmeister et al., 2011a), both of which are controlled by climate.

A major control on DCF is the extent to which the deposition of a speleothem approximates open- or closed-system conditions. Under the closed-system end member, the DIC of the percolation water is isolated from the soil-gas pCO_2 ($CO_{2,g}$) reservoir. As a consequence, the ^{14}C activity of the DIC reaching the speleothem contains a ca. 50:50 ratio of dead carbon to ~modern carbon if saturation is reached between the bedrock and the solution. This is because each mole of soil CO_2 (in bulk reservoir terms, at or close to equilibrium with the ^{14}C activity of the atmosphere) that is used in the dissolution of the bedrock (no measurable ^{14}C) creates 1 mol of radioactively dead HCO_3-. By contrast, under open-system conditions there is the possibility of $^{14}CO_2$ exchange between the percolation water DIC and the $CO_{2,g}$ reservoir, resulting in an increase in the ^{14}C activity of the DIC as the time of exchange increases (Hendy, 1971).

Notwithstanding the above complications with the DCF, a number of recent studies have used radiocarbon measurements in speleothems to explore a range of palaeoclimate problems. Beck et al. (2001), and more recently Hoffmann et al. (2010), attempted to extend the radiocarbon calibration curve using high-resolution ^{14}C measurements from U-Th dated stalagmites from the Bahamas. The authors noted large, short-term variations in DCF that were superimposed on a constant offset to the IntCal04 radiocarbon calibration curve (Reimer et al., 2004) for the period of overlap (~11–15 thousand years before present). A similar study, conducted by Southon et al. (2012) from Hulu Cave, China, also highlighted a constant offset to the more recent IntCal09 curve (Reimer et al., 2009) and, in particular, observed a relatively stable DCF through known perturbations in regional hydrology, such as the Younger Dryas. On this basis, the authors were able to extend the calibration curve by assuming a stable DCF signal. Other studies have shown that quite large and abrupt shifts in DCF can occur in response to variations in regional climate variability and soil processes above the cave. For example, using a number of speleothems from Europe, Genty et al. (2001) demonstrated that those sites with annual temperature amplitudes greater than ~7 °C exhibited a DCF decrease when temperature increased; they inferred the temperature shifts to reflect changes in SOM turnover rate. In addition, they highlighted a significant positive correlation between $\delta^{13}C$ and DCF, which was interpreted to be a direct consequence of limestone dissolution associated with open- versus closed-system conditions. Conversely, Oster et al. (2010) noted an anti-correlation between DCF and $\delta^{13}C$ in a stalagmite from California, which they interpreted to indicate that higher DCF values occurred during wetter periods (and *vice versa*) during the deglaciation to early Holocene. The authors attributed this link, between wet conditions and a high DCF, to an increased average age of the SOM during wetter intervals. A study by Fohlmeister et al. (2010) on the radiogenic and stable C isotope systematics of modern cave drip waters from Grotta Di Ernesto, Italy, revealed a pronounced annual cycle in ^{14}C of the drip water DIC in response to seasonal fluctuations in karst hydrology. As a follow-up study, Fohlmeister et al. (2011b) used a soil-karst model to explore the C isotope activity of these drip waters in greater detail. They found that major changes in the C isotope composition of the drip water occurred in response to variations in open- versus closed-system conditions along with changes in the partial pressure of $CO_{2,g}$.

In this paper, we investigate the DCF content of a tropical speleothem during a brief interval of the Holocene [~2.4 to ~2.8 thousand years before the present (ka), where "present" is defined as 1950 A.D.], marked by a prominent excursion in atmospheric radiocarbon content (McCormac et al., 2004; Reimer et al., 2004), using high-resolution accelerator mass spectrometry (AMS) ^{14}C analysis. We use a well-defined uranium-series age model and the Southern Hemisphere ^{14}C calibration curve (SHCal04; McCormac et al., 2004) to derive a DCF time series through this interval, then compare this series to stable-isotope ($\delta^{13}C$ and $\delta^{18}O$) and trace-element (Mg/Ca) data from the same speleothem (previously reported in Griffiths et al., 2009, 2010a) to determine the forcing mechanisms. In addition, we analysed ^{14}C through the bomb pulse to provide input parameters to a soil-karst model (Genty and Massault, 1999; Fohlmeister et al., 2011a), which was used to explore the initial ^{14}C activity ($a^{14}C$) in greater detail between the soil-water DIC above Liang Luar and the speleothem within the cave. Coupling the stalagmite ^{14}C measurements with the soil-karst C model allowed us to explore the degree to which each of the known C sources influenced the DCF in our speleothem. We find that the DCF variability is predominantly controlled by limestone dissolution associated with open- versus closed-system conditions, rather than kinetic fractionation and/or variations in the age spectrum of SOM. In addition, we note that over the 2.4–2.8 ka period, higher DCF values occurred during periods of higher cave recharge (inferred from $\delta^{18}O$, $\delta^{13}C$, and Mg/Ca values) and *vice versa*. We suggest that wetter (drier) periods were characterised by more closed-system (open-system) conditions in the overlying aquifer, which inhibited (promoted) gas exchange between the DIC of the karst water and soil-gas CO_2. This resulted in the incorporation of more (less) bedrock-derived dead carbon into the infiltrating water and hence into the speleothem calcite during wetter periods. A similar pattern is observed through the pre- and post-bomb intervals (~1950–2000 A.D.).

2. Study site and sample description

The stalagmite used in this study (LR06-B1), previously reported in Griffiths et al. (2009, 2010a, 2010b), was collected from Liang Luar, a ~1.7 km-long cave on the Indonesian island of Flores. The cave is situated ~550 m above mean sea-level (a.m.s.l.) and has developed within reefal (mainly built by corals) carbonates of Late Miocene-Early Pliocene age, which are mantled in part by volcanics of Quaternary age (Monk et al., 1997). The limestone host-rock contains folded strata that dip between 10 and 25° (Westaway, 2006) and is composed of a tuff-bearing dolomitic limestone with a sandy composition (van Bemmelen, 1949). The cave is overlain by ~30–50 m of bedrock, with the top 1–2 m of it representing the relatively thin soil layer. The stalagmite was collected from a large chamber ~600–800 m from the cave entrance, which is isolated from the external environment by a series of narrow passage-ways and rock falls, inhibiting air-flow and thus inducing a high relative humidity (close to 100%). Mean temperature of the chamber measured during field expeditions in 2007 and 2009 was 24.5 ± 0.5 °C, which closely resembles the mean annual temperature at the ground surface. The vegetation cover above the cave is dominated by tropical forest and coffee plantations.

The region occupying Liang Luar has an average annual rainfall of ~1200 mm. Most of the cave recharge (~69%) is delivered by the Australian-Indonesian summer monsoon, which occurs between

the months of November to March and is characterised by a replacement of the dry southeasterly trade winds (austral winter dry season) with the convective northwesterly monsoonal winds as the intertropical convergence zone moves southward over the island.

Stalagmite LR06-B1 measures ~1.25 m in length and was extracted as two sections from a large breakdown block of host bedrock that had unloaded from the cave roof (Fig. 1). Section A of the specimen was *in situ* at the time of collection in 2006 while section B had broken off and fallen about ~1.57 ka (Fig. 1). The petrography of the stalagmite is characterised by alternating layers of slightly opaque, compact-columnar calcite and translucent, open-columnar calcite (Fig. 1).

3. Methods

3.1. U-Th dating

A total of 13 pieces of calcite (11 of which weighed ~50 mg and two weighed ~300 mg) were extracted from the central growth axis of stalagmite LR06-B1 (Fig. 1). Samples were extracted using a carbide dental burr fitted to an air drill or to a micromilling lathe. $^{230}Th/^{234}U$ age determinations were obtained using both thermal ionisation mass spectrometry (TIMS) and multi-collector inductively coupled plasma mass spectrometry (MC-ICP-MS). TIMS $^{230}Th/^{234}U$ analyses were carried out at the University of Queensland, Australia, using a Fisons VG Sector 54-30 mass spectrometer equipped with

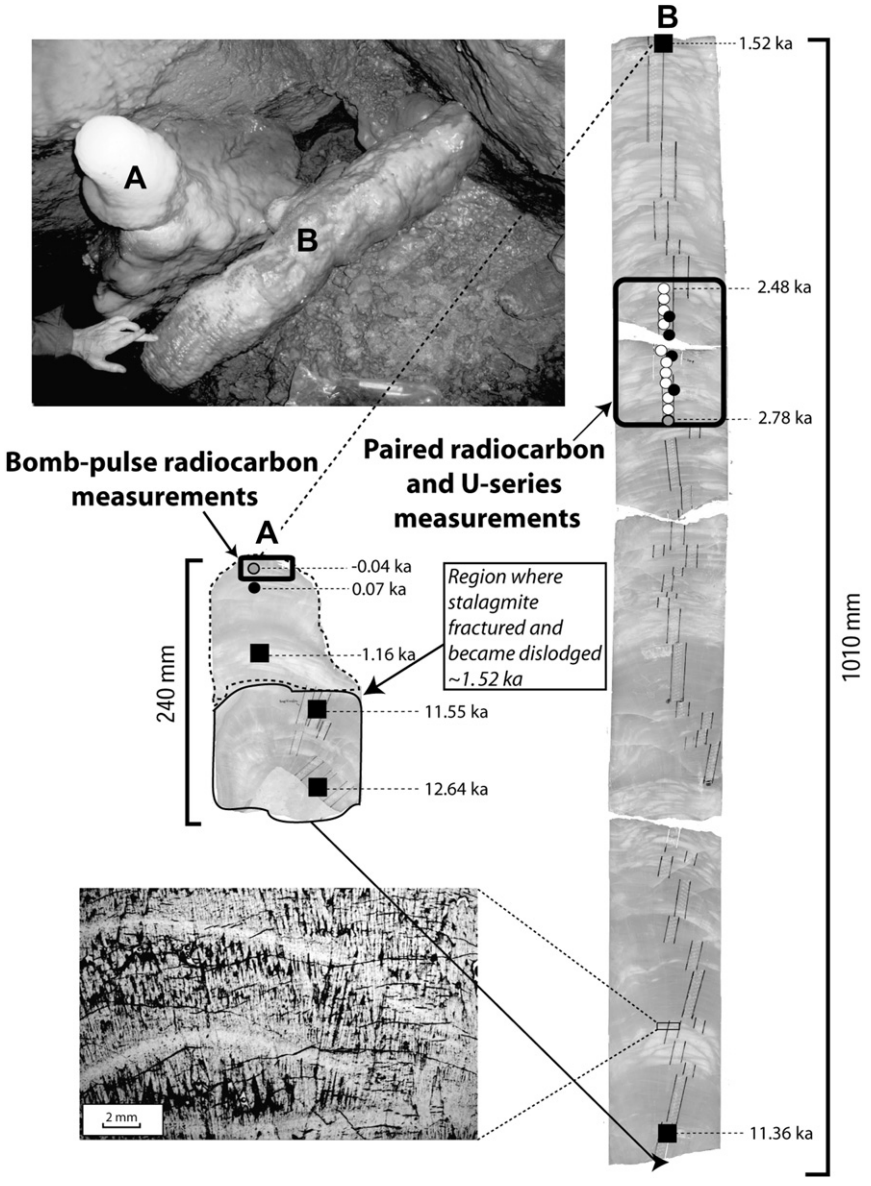

Fig. 1. Photograph of stalagmite LR06-B1 (upper left panel) prior to collection in 2006, along with scanned images of the separate calcite pieces previously analysed (Griffiths et al., 2009, 2010a, 2010b). Section A was *in situ* at the time of collection while section B was dislodged from its base ~1.52 ka before present ("present" = 1950 A.D.). The black boxes indicate the two regions of the stalagmite where samples were extracted for ^{14}C analysis and U-Th dating. The white filled circles indicate the positions of paired U-Th and ^{14}C measurements while the black filled circles represent additional ^{14}C analyses. The two grey filled circles (i.e. at −0.04 ka and 2.78 ka) show the positions of additional paired U-Th and ^{14}C measurements, though in this case the U-Th measurements were previously reported in Griffiths et al. (2009) and as such are not presented in Table 1. The black filled squares indicate the positions of U-Th dates previously reported in Griffiths et al. (2009), also not shown in Table 1. The petrographic image (lower left panel) highlights the alternating layers of slightly opaque, compact-columnar calcite and translucent, open-columnar calcite.

a WARP filter and an ion counting Daly detector, as described by Zhao et al. (2001) and Yu et al. (2006). MC-ICP-MS U-Th analyses were conducted on two separate Nu-Instruments Nu Plasma mass spectrometers housed at the University of Melbourne, Australia, and the University of Queensland. For a detailed description of the MC-ICP-MS methods employed at the University of Melbourne, we refer the reader to Hellstrom (2003), while those methods employed at the University of Queensland can be found in Zhou et al. (2011).

3.2. Stable-isotope ($\delta^{18}O$, $\delta^{13}C$) and trace-element (Mg/Ca) measurements

For the lower portion of the stalagmite, oxygen ($\delta^{18}O$) and carbon ($\delta^{13}C$) isotope values were determined from calcite powders drilled at 1-mm increments along the central growth axis of stalagmite LR06-B1 (Fig. 1). Isotope measurements were made using a GV Instruments GV2003 continuous-flow isotope ratio mass spectrometer (IRMS) at the University of Newcastle, Australia. Results are expressed as the deviation in per mil (‰) between the sample and the VPDB standard using the delta notation. The analytical uncertainty (1σ) of a working standard (a Carrara Marble called New1) was 0.08‰ for $\delta^{18}O$ and 0.05‰ for $\delta^{13}C$. These data were previously published in Griffiths et al. (2009, 2010a, 2010b).

For the modern portion of the stalagmite, the isotopes were obtained from 30 to 70 μg powders micromilled at 0.15-mm increments along the central growth axis. Measurements were carried out on a Thermo Finnigan Kiel IV Carbonate device coupled with a Delta V Plus IRMS at the University of California, Irvine. Analytical uncertainty (1σ) of the standards was 0.06‰ for $\delta^{18}O$ and for 0.03‰ for $\delta^{13}C$.

Subsamples were analysed for Mg and Ca on a Varian Liberty 4000 inductively coupled plasma atomic emission spectrometer (ICP-AES). Molar concentrations of the elements were calculated from ICP-AES intensities using four internal working standards of known concentration, and a blank, with concentrations expressed as ratios to Ca. Acid blank corrections were applied to both sample and standards data prior to conversion of the data to ratios. The relative standard deviation of replicate standards of Mg and Ca was 1.6% and 1.5%, respectively. These data were previously published in Griffiths et al. (2010a).

3.3. ^{14}C measurements

Fifteen calcite cubes weighing ~100 mg were extracted (using a carbide dental burr fitted to an air drill) every ~5 mm along the central growth axis of LR06-B1 between 345 and 422 mm (i.e. 2.4–2.8 ka) from the top of the stalagmite; of these 15 samples, 11 were splits of calcite used for U-Th dating. In addition, 21 samples, micromilled as calcite powders and weighing ~3–5 mg, were extracted at 0.15–0.45 mm increments along the growth axis from the top of the stalagmite down to a depth of 6.15 mm. Based on the U-Th age model, analysing ^{14}C activity over this depth range was sufficient to cover the bomb pulse. For the AMS ^{14}C analyses, ~3–5 mg of calcite powders (for the bomb pulse) and ~10 mg of calcite chunks (for the 2.4–2.8 ka interval) were dissolved in 2 mL 85% H_3PO_4, producing CO_2 gas that was graphitized using excess H_2 over an Fe catalyst. The graphite was then rear-pressed in an aluminium cathode for AMS measurement. For a more detailed description of these methods refer to Hua et al. (2001). It should be noted that radiocarbon ages of carbonate powders may be affected by surface contamination with modern atmospheric CO_2. However, this effect is negligible for our samples because they are quite modern (younger than 1940 A.D.).

^{14}C measurements were conducted on the 2MV HVEE "STAR" AMS in the Institute for Environmental Research, Australian Nuclear Science and Technology Organisation (ANSTO) (Fink et al., 2004). Calcite ^{14}C measurements were normalized to oxalic acid standards (HOxI and HOxII), which were interspersed for each run. ^{14}C measurements were also blank-corrected using the IAEA C1 marble procedural blank and assessed for machine background using spectroscopic-grade powdered graphite from Union Carbide Co.

4. Results

4.1. U-Th chronology

The stable-isotope, trace-element and DCF (see next section) time series for the late Holocene section of stalagmite LR06-B1, were anchored by a total of 11 U-Th dates (Fig. 2a, Table 1). In addition, the chronology for the upper section of LR06-B1, containing the ^{14}C bomb pulse (i.e. the top ~6 mm), was constrained by two U-Th dates (Fig. 2b, Table 1).

For all samples, U concentrations range from 189 to 463 ng/g, with the median being 315 ng/g. The $^{230}Th/^{232}Th$ ratios are relatively high in the majority of samples, indicating limited detrital-thorium contamination. The detrital-thorium corrected ages for the upper (i.e. modern) and lower (i.e. late Holocene) portions of the

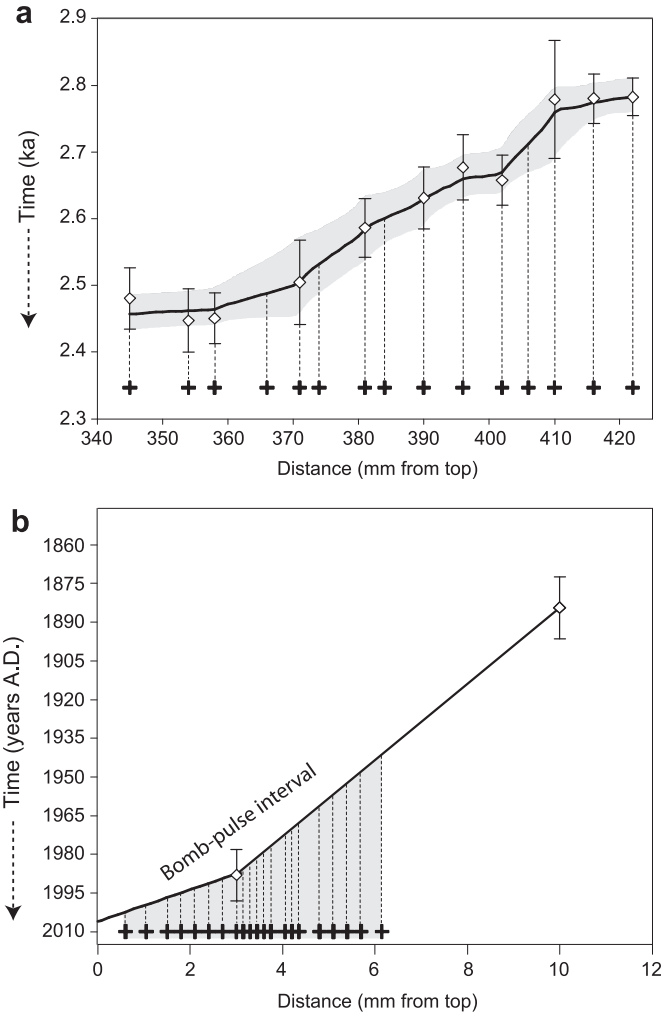

Fig. 2. U-Th age determinations for (a) the late Holocene (~2.4–2.8 ka) and (b) the instrumental (~1941–2002) period. Diamonds and attached error bars are the U-Th ages and their 95% uncertainties. Positions of the paired ^{14}C measurements (black crosses) are indicated at the bottom of each figure. The solid black lines are the U-Th age-depth models.

Table 1
TIMS and MC-ICP-MS U-Th age data (ka) for stalagmite LR06-B1 from Liang Luar.

Sample I.D.	Depth [mm]	U [ng/g]	[^{230}Th/^{232}Th]	[^{230}Th/^{238}U]	[^{234}U/^{238}U]	Uncorr. ^{230}Th age [ka]	Corr. ^{230}Th age [ka]	Corr. initial [^{234}U/^{238}U]
15/A1-2C1[a]	345	404	884.4	0.0290 ± 0.0005	1.2515 ± 0.0024	2.500 ± 0.045	2.480 ± 0.046	1.253 ± 0.002
14/A1-1B9[a]	354	315	665.8	0.0283 ± 0.0005	1.2340 ± 0.0024	2.474 ± 0.046	2.447 ± 0.046	1.236 ± 0.002
13/A1-1A7[a]	358	463	1118.8	0.0280 ± 0.0004	1.2249 ± 0.0021	2.466 ± 0.036	2.450 ± 0.037	1.227 ± 0.002
11/A1-1C2[a]	371	189	805.1	0.0293 ± 0.0007	1.2516 ± 0.0025	2.526 ± 0.062	2.504 ± 0.063	1.253 ± 0.002
9/B1-6A11[a]	381	307	1133.1	0.0302 ± 0.0005	1.2543 ± 0.0022	2.601 ± 0.045	2.585 ± 0.045	1.256 ± 0.002
7/B1-6A8[a]	390	288	563.9	0.0305 ± 0.0005	1.2380 ± 0.0020	2.664 ± 0.046	2.630 ± 0.046	1.240 ± 0.002
6/B1-6C5[a]	396	440	268.2	0.0317 ± 0.0005	1.2483 ± 0.0023	2.749 ± 0.045	2.676 ± 0.050	1.250 ± 0.002
5/B1-6A4[a]	402	402	1711.2	0.0303 ± 0.0004	1.2275 ± 0.0026	2.669 ± 0.037	2.658 ± 0.037	1.229 ± 0.003
3/B1-5A18[a]	410	294	1028.3	0.0322 ± 0.0010	1.2464 ± 0.0025	2.797 ± 0.089	2.777 ± 0.089	1.248 ± 0.003
2/B1-5A16[a]	416	421	1225.4	0.0319 ± 0.0004	1.2353 ± 0.0021	2.797 ± 0.037	2.780 ± 0.037	1.237 ± 0.002
1/B1-5B14[b]	422	451	735.6	0.0322 ± 0.0003	1.2413 ± 0.0027	2.810 ± 0.028	2.783 ± 0.029	1.243 ± 0.003
B1-E1/03[b]	3.0	292	10.9	0.0006 ± 0.00004	1.2526 ± 0.0019	−0.005 ± 0.003	−0.039 ± 0.010	1.254 ± 0.002
B1-E1/10[c]	10.0	290	32.5	0.0018 ± 0.00007	1.2440 ± 0.0011	0.102 ± 0.006	0.067 ± 0.012	1.244 ± 0.001

"Depth [mm]" is the distance from the top of the stalagmite. Ages are reported in thousands of years before present (ka), where "present" = 1950 A.D. Activity ratios (in brackets) were determined by the methods described in Hellstrom (2003) and supplementary materials of Drysdale et al. (2005). Corrected (Corr.) ^{230}Th ages were calculated using Eq. (1) of Hellstrom (2006), assuming non-radiogenic ^{230}Th/^{232}Th = 7 ± 2 [calculated using the method of Hellstrom (2006)], and half-lives specified in Cheng et al. (2000).

[a] Dates determined by MC-ICP-MS at the University of Melbourne, Australia.
[b] Date determined by TIMS at the University of Queensland, Australia. These data were published in Griffiths et al. (2009).
[c] Date determined by MC-IPC-MS at the University of Queensland, Australia.

stalagmite all lie in stratigraphical order (within 2σ dating uncertainty). The age-depth models for both portions of the record were constructed by means of Bayesian-Monte Carlo simulations using the Wavemetrics Igor Pro software package. A more detailed description of the technique is given in Drysdale et al. (2005, 2007).

4.2. Radiocarbon activity and dead carbon fraction (DCF)

The radiocarbon activity through the upper and lower portions of the stalagmite is shown in Table 2. The a^{14}C values represent the initial ^{14}C activity of the speleothem calcite, which is defined by:

$$a^{14}C_{stal.init.} = a^{14}C_{meas.}/\exp[(-\ln(2)/5730) \times t]$$

where a^{14}C$_{meas.}$ is the measured calcite ^{14}C activity and t is the U-Th age of the calcite in calendar years before present (cal. B.P.).

For the lower portion of the speleothem, the a^{14}C initial activity ranges from 81.2 ± 0.3 to 83.4 ± 0.3 pMC and averages 82.5 pMC over the ~2.4–2.8 ka period. The pattern of a^{14}C variability during this interval broadly follows, but plots below, the contemporaneous SHCal04 atm curve (McCormac et al., 2004) (Fig. 3). This offset between the atmosphere and a^{14}C in the speleothem reflects the dilution effect (DE) of radioactively 'dead' carbon from the limestone host rock and/or older C from soil organic matter. The speleothem a^{14}C profile through the bomb pulse has pre-bomb (i.e. prior to ~1955 A.D.) values of between 78.4 ± 0.5 and 79.3 ± 0.5 pMC while final values plateau between 80.8 ± 0.5 and 83.5 ± 0.4 pMC (Fig. 4). The a^{14}C initial values peak at 1984–1989 A.D. where values range between 82.4 and 83.5 pMC.

To quantify the amount of 'dead' carbon incorporated into the upper and lower portions of speleothem LR06-B1, we calculated the DCF following the methods of Genty et al. (1999), where:

$$DCF(\%) = \left[1 - \left(a^{14}C_{stal.init.}/a^{14}C_{atm.init.}\right)\right] \times 100$$

where a^{14}C$_{atm.init.}$ is the atmospheric a^{14}C initial activity, derived from the SHCal04 calibration curve (McCormac et al., 2004) for the period before 1950 A.D., from tree-ring data (Hua et al., 2000, 2003) for the interval between 1950 and 1954 A.D., and from the updated SH zone (Hua and Barbetti, 2004) for the period from 1955 A.D. onwards. To calculate the DCF and associated 1σ error, we first calculated the a^{14}C$_{atm.init.}$ at the time of each stalagmite ^{14}C measurement using a Monte Carlo (MC) approach. This was achieved as follows: (i) first we imported the SH calibration curve, then generated 10,000 Gaussian distributed ages around the U-Th age at the depth of each ^{14}C measurement (with mean and 1σ as given by the age model); (ii) for each of the 10,000 MC ages, the mean a^{14}C$_{atm.init.}$ activity, plus the according 1σ deviation, was derived using linear interpolation between the values given in the SH04 calibration curve; (iii) we then randomly chose one value within the mean and 1σ error of the a^{14}C$_{atm.init.}$ activity, as previously determined; (iv) finally, we took the mean of the 10,000 a^{14}C$_{atm.init.}$ activity values and calculated the 1σ standard deviation.

The inferred DCF values are displayed in Tables 2and 3, and Figs. 5–8. Through the ~2.4–2.8 ka interval, *total* DCF values range between ~15.7% and ~19.4% while DCF from host rock contribution only (DCF$_{host\ rock}$; see next section) ranges between ~17.2% and ~19.5%. By contrast, DCF$_{host\ rock}$ during the instrumental period (~1940–2000 A.D.) ranges between ~20.6% and ~22.6%. The reason for this apparent ~3–5% offset in DCF between the late Holocene and instrumental period may be due to a slight shift in the flow route of the karst water feeding the stalagmite, such that the system is in a more closed state today. It is possible that tectonic activity, as evidenced from the broken section (i.e. Section B, Fig. 1) of stalagmite LR06-B1 that was dislodged ~1.57 ka, may have redirected the flow route of the karst water and with it, the carbonate dissolution conditions.

5. Discussion

Notwithstanding the fractionation effects inside the cave during calcite precipitation, the initial ^{14}C activity of DIC in the soil-water, and hence the speleothem calcite, is typically dominated by two main end members: (i) the ^{14}C of the soil CO_2, which is controlled by the decomposition of SOM and plant respiration; and (ii) the C originating from the dissolution of the carbonate host rock, which is typically devoid of any ^{14}C.

In regard to the first end member, the ^{14}C of the total $CO_{2,g}$ is controlled by a mixture of ^{14}C inputs from plant respiration, which has a ^{14}C activity similar to that of the atmosphere, and the decomposition of SOM, which introduces CO_2 with a signature of past atmospheric ^{14}C activity minus the small amount of radioactive decay since the time of OM burial. Although, given both the relatively short turnover time of SOM (Trumbore, 2000) and the

Table 2
The ^{14}C data and associated 1σ errors for the upper (~1941–2002 A.D.) and lower (~2.4–2.8 ka) sections of stalagmite LR06-B1, as indicated in Fig. 1. Ages of the ^{14}C measurements are based on the U-Th age model. U-Th ages in brackets for the modern samples are displayed in years A.D.

Sample I.D.	Lab ID	Depth [mm]	U-Th age model [ka]	$a^{14}C_{meas.}$ [pMC]	$a^{14}C_{stal.init.}$ [pMC]	$a^{14}C_{atm.init.}$ [pMC]	Total DCF [%]
15/A1-2C1	OZL244	345	2.456	60.84 ± 0.24	81.89 ± 0.32	98.73 ± 0.36	17.06 ± 0.45
14/A1-1B9	OZL243	354	2.461	61.30 ± 0.23	82.55 ± 0.31	98.75 ± 0.37	16.40 ± 0.44
13/A1-1A7	OZL242	358	2.463	61.19 ± 0.23	82.43 ± 0.31	98.75 ± 0.37	16.53 ± 0.45
12/A1-1A5	OZL241	366	2.486	61.63 ± 0.24	83.25 ± 0.32	98.77 ± 0.43	15.72 ± 0.49
11/A1-1C2	OZL240	371	2.504	60.29 ± 0.23	81.62 ± 0.31	98.82 ± 0.42	17.40 ± 0.47
10/A1-1A1	OZL239	374	2.531	59.77 ± 0.22	81.18 ± 0.30	98.96 ± 0.35	17.97 ± 0.42
9/B1-6A11	OZL238	381	2.582	60.31 ± 0.24	82.42 ± 0.33	99.52 ± 0.35	17.18 ± 0.44
8/B1-6C9	OZL237	384	2.599	60.93 ± 0.24	83.44 ± 0.33	99.75 ± 0.39	16.36 ± 0.46
7/B1-6A8	OZL236	390	2.628	60.43 ± 0.23	83.04 ± 0.32	100.16 ± 0.45	17.09 ± 0.47
6/B1-6C5	OZL235	396	2.658	58.86 ± 0.23	81.18 ± 0.32	100.74 ± 0.41	19.41 ± 0.45
5/B1-6A4	OZL234	402	2.668	60.22 ± 0.23	83.16 ± 0.32	100.84 ± 0.40	17.54 ± 0.45
4/B1-6C2	OZL233	406	2.711	59.48 ± 0.21	82.56 ± 0.29	100.64 ± 0.73	17.96 ± 0.66
3/B1-5A18	OZL232	410	2.758	59.65 ± 0.21	83.27 ± 0.29	99.90 ± 1.14	16.65 ± 0.99
2/B1-5A16	OZL231	416	2.773	59.38 ± 0.23	83.06 ± 0.32	99.53 ± 0.71	16.56 ± 0.67
1/B1-5B14	OZL230	422	2.781	58.59 ± 0.22	82.02 ± 0.31	99.43 ± 0.62	17.51 ± 0.60
B1-4	OZO063	0.60	−0.052 (2002)	82.23 ± 0.50	81.71 ± 0.50	108.39 ± 2.62	24.62 ± 1.88
B1-7	OZN246	1.05	−0.050 (2000)	82.27 ± 0.44	81.78 ± 0.44	109.65 ± 3.03	25.42 ± 2.10
B1-10	OZO064	1.50	−0.047 (1997)	82.01 ± 0.49	81.55 ± 0.49	111.31 ± 3.50	26.73 ± 2.34
B1-12	OZN247	1.80	−0.045 (1995)	82.21 ± 0.50	81.76 ± 0.50	112.52 ± 3.80	27.34 ± 2.49
B1-14	OZO065	2.10	−0.043 (1993)	81.55 ± 0.42	81.13 ± 0.42	114.06 ± 4.18	28.87 ± 2.63
B1-16	OZN248	2.40	−0.041 (1991)	81.83 ± 0.54	81.42 ± 0.54	115.52 ± 4.53	29.52 ± 2.80
B1-18	OZO066	2.70	−0.039 (1989)	83.30 ± 0.46	82.91 ± 0.46	117.35 ± 4.96	29.35 ± 3.01
B1-20	OZO067	3.00	−0.038 (1988)	83.24 ± 0.46	82.86 ± 0.46	119.13 ± 5.55	30.44 ± 3.26
B1-21	OZO068	3.15	−0.036 (1986)	82.78 ± 0.50	82.41 ± 0.50	120.81 ± 6.10	31.79 ± 3.47
B1-22	OZN249	3.30	−0.034 (1984)	83.88 ± 0.38	83.53 ± 0.38	123.46 ± 6.88	32.34 ± 3.78
B1-23	OZO069	3.45	−0.032 (1982)	82.15 ± 0.36	81.84 ± 0.36	127.09 ± 8.04	35.61 ± 4.08
B1-24	OZO070	3.60	−0.029 (1979)	82.08 ± 0.36	81.79 ± 0.36	131.16 ± 9.31	37.64 ± 4.43
B1-25	OZN250	3.75	−0.027 (1977)	81.67 ± 0.54	81.40 ± 0.54	135.24 ± 10.10	39.81 ± 4.51
B1-27	OZN251	4.05	−0.023 (1973)	81.35 ± 0.45	81.13 ± 0.45	143.43 ± 11.35	43.44 ± 4.49
B1-28	OZO071	4.20	−0.021 (1971)	81.50 ± 0.40	81.29 ± 0.40	145.36 ± 12.95	44.08 ± 4.99
B1-29	OZN252	4.35	−0.018 (1968)	82.65 ± 0.46	82.47 ± 0.46	144.70 ± 16.47	43.01 ± 6.50
B1-32	OZN253	4.80	−0.012 (1962)	80.92 ± 0.45	80.81 ± 0.45	124.60 ± 22.22	35.15 ± 11.57
B1-34	OZN254	5.10	−0.007 (1957)	79.40 ± 0.46	79.33 ± 0.46	108.73 ± 15.29	27.04 ± 10.27
B1-36	OZO072	5.40	−0.002 (1952)	79.14 ± 0.37	79.12 ± 0.37	100.68 ± 7.30	21.41 ± 5.71
B1-38	OZN255	5.70	0.002 (1948)	78.39 ± 0.49	78.41 ± 0.49	98.48 ± 2.68	20.38 ± 2.23
B1-41	OZN256	6.15	0.009 (1941)	78.66 ± 0.46	78.74 ± 0.46	98.18 ± 0.31	19.80 ± 0.53

relatively small ^{14}C fractionation from gaseous CO_2 to DIC, the ^{14}C in the soil-water DIC should reflect that of the atmosphere (Fohlmeister et al., 2011a), except during periods of large and abrupt changes in atmospheric ^{14}C (Trumbore, 2000). The degree to which each of these soil reservoirs (i.e. both the decay of SOM and plant respiration) contributes to the total $CO_{2,g}$ pool can vary throughout the year depending on the vegetation cycle above the cave (Dörr and Münnich, 1986).

The other dominant control on the initial ^{14}C content of speleothems is the dissolution of the karst limestone as infiltrating meteoric waters mix with the host rock. As the host limestone is devoid of any ^{14}C, the relative contribution of 'dead' C from this reservoir, to the total C pool of the percolating groundwater, largely influences the final ^{14}C activity of the speleothem calcite. In theory, dissolution can occur under two end member situations (open- or closed-system dissolution) (Hendy, 1971). However, in the real soil-karst environment, carbonate dissolution is likely to occur under an intermediate state between a completely open and a completely closed-system (Rudzka et al., 2011). Under the open-system end member, the DIC maintains isotopic equilibrium with the unlimited reservoir of $CO_{2,g}$. By contrast, under a closed-system isotopic equilibrium between the DIC and $CO_{2,g}$ is not maintained, and thus the soil-water DIC accrues higher $\delta^{13}C$ and lower $a^{14}C$ values during limestone dissolution (Hendy, 1971). Therefore, a change to a more open (closed) carbonate dissolution system would typically result in higher (lower) ^{14}C activities and lower (higher) $\delta^{13}C$ values in the vadose zone and ultimately cave interior.

One last important influence on speleothem C isotopes is disequilibrium isotope fractionation, which mainly occurs during calcite precipitation. This process is generally governed by drip rates and/or the degree of cave ventilation (Mühlinghaus et al., 2009; Scholz et al., 2009), both of which can be controlled by climate. For example, drier conditions can result in a lower drip rate, which can increase the $\delta^{13}C$ values due to the longer time available for calcite precipitation between successive drips (Mühlinghaus et al., 2009; Scholz et al., 2009; Dreybrodt and Scholz, 2011). Dry conditions can also favour disequilibrium fractionation at and/or 'upstream' of the drip site during prior calcite precipitation (PCP) (Fairchild et al., 2000; Fairchild and Treble, 2009), a process by which CO_2 degassing causes preferential loss of the lighter ^{12}C isotope to the gas phase and hence enriches the percolation water, and ultimately the speleothem, in ^{13}C. Another process affecting the C isotopes is fractionation between gaseous CO_2 and HCO_3^- (in the aquifer) and HCO_3^- and $CaCO_3$ (during calcite precipitation).

In the following sections, we take a soil-karst modelling approach, similar to that of Genty and Massault (1999), to examine the sources and processes that control the initial ^{14}C, and hence DCF, in stalagmite LR06-B1. Coupling the soil-karst model with real data enables us to: (i) correct the DCF for SOM/vegetation influences and fractionation effects, for both the late Holocene (2.4–2.8 ka) and instrumental (~1940–2000) periods, by separating the single effects on speleothem ^{14}C; (ii) demonstrate that the level of host rock contribution (open/closed carbonate dissolution) is responsible for the changes in DCF; (iii) test whether open or closed-system carbonate dissolution is triggered by precipitation amount, as inferred from $\delta^{18}O$ and Mg/Ca results; and (iv) explain the $\delta^{13}C$ excursions during the late Holocene.

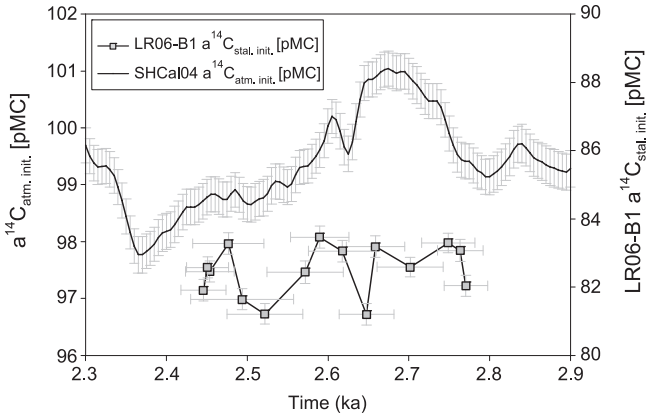

Fig. 3. The initial ^{14}C activity of the atmosphere (SHCal04) compared with the initial ^{14}C activity of speleothem LR06-B1 (grey squares) during the late Holocene. Horizontal error bars on the speleothem samples represent the width of the microdrilled area converted to an age, while the vertical error bars represent 1-σ uncertainty in the ^{14}C measurements.

5.1. Separating the DCF components in stalagmite LR06-B1

In order to disentangle the different contributions to DCF during the 2.8 and 2.4 ka period, we first focus on the influence of SOM and vegetation. Following this, we calculate the contribution of C isotope fractionation between $CO_{2,g}$ and bicarbonate (the main component of DIC). Finally, we differentiate between the host rock contribution and fractionation processes between HCO_3^- and $CaCO_3$ inside the cave, with support of measured stable C isotopes.

5.1.1. Estimating the age spectrum of SOM above Liang Luar

With the use of a soil-host rock-cave model for C isotopes, first proposed by Genty et al. (1999), we estimate the age spectrum of SOM above Liang Luar by analysing the radiocarbon bomb pulse detected in LR06-B1 (Fig. 4). The model describes the total $CO_{2,g}$ composition as contributions from three main SOM reservoirs (c_1, c_2, c_3 with $\Sigma c = 1$) of different ages (y_1, y_2, y_3); this includes a fast (y_1), medium (y_2) and slow (y_3) reservoir. The main step in the model is that total soil-gas ^{14}C ($a^{14}C_g$) is calculated by:

$$a^{14}C_g = c_1 \times \left(a^{14}Cy_1\right) + c_2 \times \left(a^{14}Cy_2\right) + c_3 \times \left(a^{14}Cy_3\right)$$

where $a^{14}Cyi$ ($i = 1, 2, 3$) are the mean decay-corrected atmospheric ^{14}C activities.

Each SOM reservoir contributes a $^{14}CO_2$ signature to the bulk $CO_{2,g}$, which is incorporated into the soil from the atmosphere by photosynthesis at the time of plant growth and modulated by radioactive decay. The $CO_{2,g}$ is adsorbed by infiltrating meteoric water and then converted to HCO_3^- (the main component of the initial DIC), leading to ^{14}C isotopic fractionation of $\sim$+1.8 pMC at a mean temperature of 25 °C using fractionation factors given by Mook and de Vries (2000) and $^{14}\varepsilon = 2.3 \times {}^{13}\varepsilon$ (Salièges and Fontes, 1984). In the next step, the ^{14}C of the initial DIC is diluted with the host rock C. The contribution of the host rock to the DIC is assumed constant through this short period. Finally, fractionation occurs between the calcite-saturated solution and precipitating calcite forming the stalagmite. For a more detailed description of the model, the reader is referred to Fohlmeister et al. (2011a).

The model parameters used to derive the SOM age spectrum were determined using an iterative process consisting of two steps. First, the fraction of dead carbon originating from the host rock was calculated by taking the mean difference between the atmospheric ^{14}C activity and the stalagmite ^{14}C measurements at the depths corresponding to the years A.D. 1941–1957. This was conducted with an *a priori,* but reasonable, estimation of y_i and c_i, based on studies estimating soil parameters with a similar vegetation cover; in this period of almost constant atmospheric ^{14}C activities, the choice of the age spectrum parameters led to a constant offset. Next, using this 'initial' host rock dead carbon value, the age spectrum of SOM was determined using the ^{14}C measurements of the stalagmite through the bomb pulse between1957 and 1980. The parameters y_i and c_i are found by minimization of the deviation between the model data set and the ^{14}C measurements of the stalagmite through the bomb- pulse period. Following this, it was necessary to re-evaluate the host rock dead carbon due to changes in the vegetation-induced dead carbon. Next, the vegetation parameters were adjusted again, and the iteration was continued until the deviations of the model output were minimized with respect to the ^{14}C values measured in the stalagmite (Fohlmeister et al., 2011a).

Using the above approach, the bomb pulse is reproduced when the host rock fraction equals 20.84% and the best-parameterized SOM age spectrum to fit the ^{14}C measurements equals:

- $y_1 = 1$ year; $c_1 = 5\%$
- $y_2 = 52$ years; $c_2 = 15\%$
- $y_3 = 280$ years; $c_3 = 80\%$

As observed in Genty et al. (1999), Fohlmeister et al. (2011a) and Hodge et al. (2011), the fit yields satisfying results (Fig. 4), although there is significant scatter around the fit; we will discuss the reason for this scatter in Section 5.2.2. These findings suggest that there is a rather old C reservoir swamping the $CO_{2,g}$ contribution from the much smaller, younger SOM reservoirs.

By using the above values, we can apply the modern age spectrum of SOM to the late Holocene (2.4–2.8 ka) section of LR06-B1, assuming a relatively constant vegetation cover for the last 3 ka. This assumption has some support from palynological studies conducted on the Indonesian islands, which suggest that vegetation characteristics in the region were relatively constant during

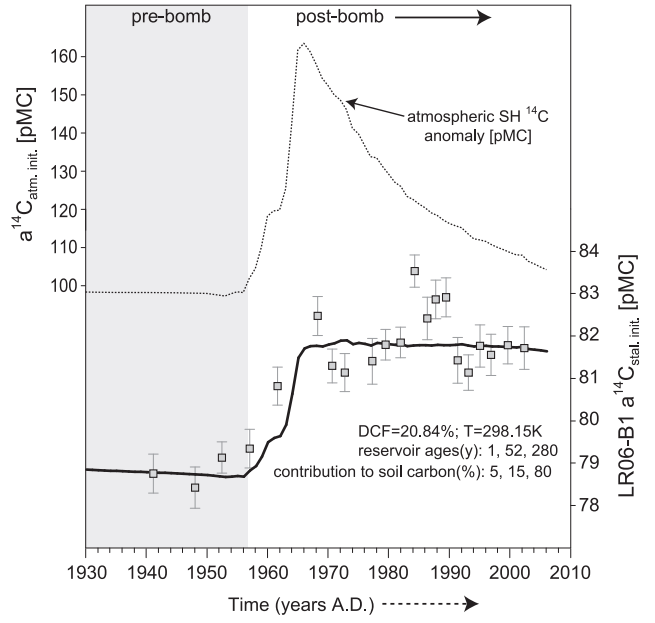

Fig. 4. Comparison of the Southern Hemisphere atmospheric ^{14}C activity (dashed line; McCormac et al., 2004) with the speleothem ^{14}C (grey squares) through the pre-and post-bomb intervals. The solid line depicts the best-modelled fit of the measured data. Values in the lower panel represent the 6 SOM parameters, the host rock contribution, and temperature (T) used to calculate the best fit (see Sec. 5.1.1). The age uncertainty of each stalagmite ^{14}C measurement (not depicted in the figure) is ±10 years based on the U-Th age-depth model.

Table 3
The dead carbon fraction (DCF) data and associated 1σ errors for the upper (~1941–2002 A.D.) and lower (~2.4–2.8 ka) sections of stalagmite LR06-B1. The data represent the *total* DCF values (3rd column from left) that exclude vegetation/SOM influences (DCF w/o veg. [%]) and fractionation effects from gaseous CO_2 to HCO_3^- (DCF w/o $CO_2 \rightarrow HCO_3^-$ fract. [%]). Also shown is the DCF contribution from the host rock only (Host rock DCF [%]). The three far right columns show calculated initial drip water $\delta^{13}C$, measured stalagmite $\delta^{13}C$, and the difference between the two ($\Delta\delta^{13}C$). U-Th ages in brackets for the modern samples are displayed in years A.D.

Sample I.D.	U-Th age model [ka]	*total* DCF [%]	DCF w/o veg. [%]	DCF w/o $CO_2 \rightarrow HCO_3^-$ fract. [%]	Host rock DCF [%]	Drip water $\delta^{13}C$ [‰]	Stal. $\Delta^{13}C$ [‰]	$\Delta\delta^{13}C$
15/A1-2C1	2.456	17.06 ± 0.45	16.48 ± 0.43	18.00 ± 0.42	18.57 ± 0.43	−14.35	−12.00	2.36
14/A1-1B9	2.461	16.40 ± 0.44	15.82 ± 0.43	17.35 ± 0.42	17.90 ± 0.42	−14.45	−12.15	2.30
13/A1-1A7	2.463	16.53 ± 0.45	15.96 ± 0.43	17.49 ± 0.42	18.10 ± 0.42	−14.42	−11.89	2.53
12/A1-1A5	2.486	15.72 ± 0.49	15.19 ± 0.47	16.74 ± 0.46	17.41 ± 0.46	−14.52	−11.68	2.84
11/A1-1C2	2.504	17.40 ± 0.47	16.89 ± 0.47	18.40 ± 0.46	18.98 ± 0.46	−14.30	−11.89	2.41
10/A1-1A1	2.531	17.97 ± 0.42	17.38 ± 0.47	18.89 ± 0.45	19.45 ± 0.45	−14.23	−11.85	2.38
9/B1-6A11	2.582	17.18 ± 0.44	16.17 ± 0.50	17.69 ± 0.49	18.35 ± 0.49	−14.39	−11.49	2.90
8/B1-6C9	2.599	16.36 ± 0.46	15.12 ± 0.50	16.68 ± 0.49	17.39 ± 0.49	−14.53	−11.41	3.11
7/B1-6A8	2.628	17.09 ± 0.47	15.49 ± 0.49	17.03 ± 0.48	17.74 ± 0.48	−14.48	−11.39	3.09
6/B1-6C5	2.658	19.41 ± 0.45	17.33 ± 0.48	18.83 ± 0.48	19.41 ± 0.47	−14.23	−11.81	2.42
5/B1-6A4	2.668	17.54 ± 0.45	15.29 ± 0.50	16.83 ± 0.49	17.58 ± 0.49	−14.50	−11.22	3.28
4/B1-6C2	2.711	17.96 ± 0.66	15.74 ± 0.52	17.28 ± 0.51	18.02 ± 0.51	−14.44	−11.26	3.18
3/B1-5A18	2.758	16.65 ± 0.99	14.97 ± 0.61	16.52 ± 0.60	17.24 ± 0.58	−14.56	−11.41	3.15
2/B1-5A16	2.773	16.56 ± 0.67	15.17 ± 0.48	16.71 ± 0.47	17.39 ± 0.47	−14.53	−11.61	2.92
1/B1-5B14	2.781	17.51 ± 0.60	16.23 ± 0.46	17.75 ± 0.45	18.46 ± 0.45	−14.38	−11.35	3.03
B1-4	−0.052 (2002)	24.62 ± 1.88	19.62 ± 0.51	21.03 ± 0.50	22.00 ± 0.50	−13.85	−9.46	4.39
B1-7	−0.050 (2000)	25.42 ± 2.10	19.57 ± 0.45	20.99 ± 0.44	21.90 ± 0.44	−13.87	−9.77	4.10
B1-10	−0.047 (1997)	26.73 ± 2.34	19.82 ± 0.50	21.23 ± 0.49	21.96 ± 0.49	−13.86	−10.58	3.28
B1-12	−0.045 (1995)	27.34 ± 2.49	19.62 ± 0.51	21.04 ± 0.50	21.74 ± 0.50	−13.89	−10.74	3.15
B1-14	−0.043 (1993)	28.87 ± 2.63	20.25 ± 0.43	21.65 ± 0.42	22.32 ± 0.42	−13.80	−10.89	2.91
B1-16	−0.041 (1991)	29.52 ± 2.80	19.97 ± 0.55	21.38 ± 0.54	22.05 ± 0.54	−13.84	−10.83	3.01
B1-18	−0.039 (1989)	29.35 ± 3.01	18.51 ± 0.47	19.95 ± 0.46	20.79 ± 0.46	−14.03	−10.23	3.80
B1-20	−0.038 (1988)	30.44 ± 3.26	18.57 ± 0.47	20.00 ± 0.46	21.06 ± 0.46	−13.99	−9.19	4.80
B1-21	−0.036 (1986)	31.79 ± 3.47	19.01 ± 0.51	20.43 ± 0.50	21.54 ± 0.50	−13.92	−8.93	4.99
B1-22	−0.034 (1984)	32.34 ± 3.78	17.91 ± 0.40	19.36 ± 0.39	20.56 ± 0.39	−14.07	−8.62	5.45
B1-23	−0.032 (1982)	35.61 ± 4.08	19.58 ± 0.38	21.00 ± 0.37	22.16 ± 0.37	−13.83	−8.55	5.28
B1-24	−0.029 (1979)	37.64 ± 4.43	19.63 ± 0.38	21.05 ± 0.38	22.24 ± 0.38	−13.82	−8.45	5.37
B1-25	−0.027 (1977)	39.81 ± 4.51	20.02 ± 0.57	21.42 ± 0.55	22.58 ± 0.55	−13.77	−8.54	5.23
B1-27	−0.023 (1973)	43.44 ± 4.49	20.19 ± 0.64	21.60 ± 0.62	22.46 ± 0.62	−13.76	−9.89	3.87
B1-28	−0.021 (1971)	44.08 ± 4.99	19.91 ± 0.77	21.32 ± 0.75	22.10 ± 0.75	−13.80	−10.26	3.54
B1-29	−0.018 (1968)	43.01 ± 6.50	18.49 ± 1.03	19.91 ± 1.01	20.74 ± 1.01	−13.97	−10.29	3.68
B1-32	−0.012 (1962)	35.15 ± 11.57	18.80 ± 1.32	20.26 ± 1.28	21.34 ± 1.26	−14.01	−9.28	4.73
B1-34	−0.007 (1957)	27.04 ± 10.27	19.43 ± 0.96	20.90 ± 0.94	21.90 ± 0.96	−13.93	−9.71	4.22
B1-36	−0.002 (1952)	21.41 ± 5.71	19.28 ± 0.58	20.75 ± 0.54	21.72 ± 0.55	−13.92	−9.68	4.24
B1-38	0.002 (1948)	20.38 ± 2.23	19.91 ± 0.53	21.38 ± 0.52	22.31 ± 0.52	−13.81	−9.76	4.05
B1-41	0.009 (1941)	19.80 ± 0.53	19.61 ± 0.48	21.07 ± 0.47	22.01 ± 0.47	−13.85	−9.81	4.04

the (late) Holocene (Western Java: Van Der Kaars et al., 2001; South Sulawesi: Hope, 2001; Western Borneo: Anshari et al., 2001). We must acknowledge, however, that the region may have undergone some vegetative alteration given the presence of coffee plantations, thus presenting a caveat to our model. However, a change in vegetation does not imply that the age spectrum of the SOM changed dramatically. Moreover, even if the age spectrum was shifted to some extent, the smoothing of the atmospheric ^{14}C signal will still be present. This is because atmospheric smoothing is generally more pronounced if the age of the vegetation above the cave is older (Fohlmeister et al., 2011a), and coffee plantations would certainly be younger than the native forest. Also, the most likely points of infiltration into the cave were occupied by native forest, suggesting little alteration above the drainage zone.

With the known SOM age spectrum and same $CO_{2,g}$ as in the modern soil, we can calculate past $^{14}CO_{2,g}$ (Fig. 5a, thick black curve). Fractionation between $CO_{2,g}$ and bicarbonate is responsible for slight C isotope enrichment (Fig. 5a, thick grey curve). The C isotope shift is constant with time as long as temperature remained stable; this is a valid assumption given that there is no evidence from marine (e.g. Stott et al., 2004; Abram et al., 2009) and terrestrial (e.g. Griffiths et al., 2010b) records to suggest that there was a significant temperature shift during this period.

The resulting DCF values for the different ^{14}C curves displayed in Fig. 5a are shown in Fig. 5b. The *total* DCF (dashed line with crosses) was calculated from the stalagmite ^{14}C data and atmospheric SHCal04 ^{14}C values. This DCF includes all effects: SOM/vegetation, isotope fractionation between gaseous CO_2 and HCO_3^-, host rock contribution, and fractionation in the cave between HCO_3^- and $CaCO_3$. The black curve with open circles shows DCF excluding the influences of SOM/vegetation and the grey curve with open triangles represents DCF that is only due to host rock contribution and fractionation in the cave. DCF only due to host rock contribution (black line with open squares) is discussed in the next section. The errors for these other DCFs (i.e. DCF without vegetation/SOM, DCF without $CO_2 \rightarrow HCO_3^-$ fractionation, and host rock only DCF) was calculated as follows: (i) first, the model (as described at the beginning of this section) calculated a time series of soil-gas ^{14}C and ^{14}C of the DIC, which is in chemical and isotopic equilibrium with the soil-gas [Fig. 5a (black and grey solid lines)]. For both time series, we calculated an 'error envelope' derived by the atmospheric ^{14}C; (ii) we then used a simple Gaussian error propagation from atmospheric values over ^{14}C decay of old vegetation, mixing of CO_2 of the vegetation compartments with different ages, and finally fractionation; (iii) after calculation of both time series and the corresponding error band, we used the same procedure, as that used to calculate the error for the *total* DCF (previously described in Section 4.2), to derive the error for the other DCFs. Hence, for all DCF errors, the uncertainty of the ^{14}C measurements, U-Th ages, and ^{14}C curves are taken into account.

5.1.2. Host rock contribution to DCF

For the 2.4 to 2.8 ka interval, we have now separated vegetation and fractionation influences on the DCF (Fig. 5b, grey curve with

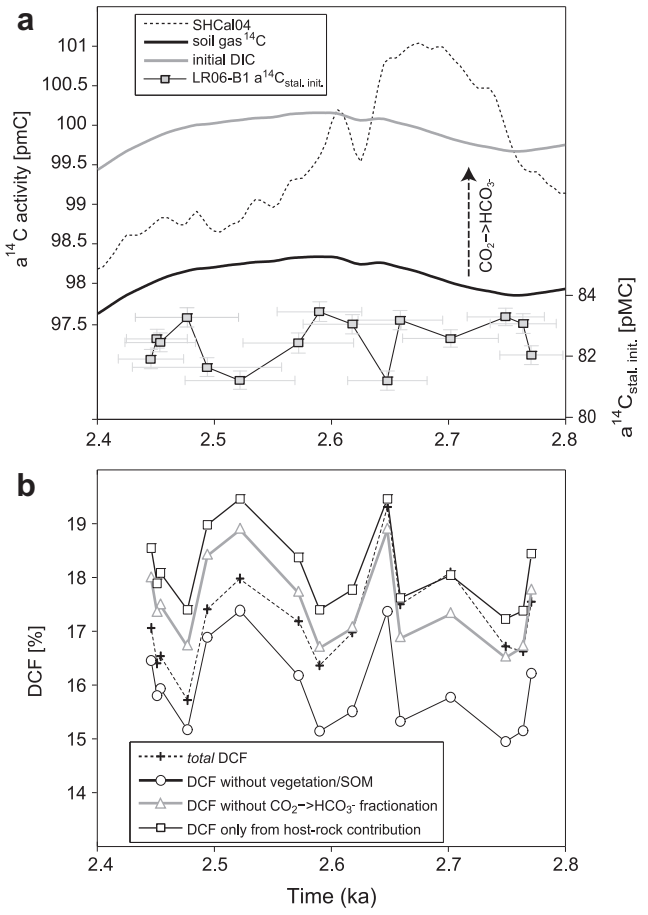

Fig. 5. (a) SHCal04 (dashed line; McCormac et al., 2004) and the modelled ^{14}C of the soil-gas (solid black line) above Liang Luar Cave using the 6 SOM parameters established through the bomb pulse. The solid grey line indicates the ^{14}C activity of the initial DIC, meaning that fractionation between gaseous CO_2 and HCO_3- would shift the ^{14}C level from the soil-gas to DIC by ~+1.8 pMC at a mean temperature of 25 °C using fractionation factors given by Mook and de Vries (2000) and $^{14}\varepsilon = 2.3 \times {}^{13}\varepsilon$ (Salièges and Fontes, 1984). The grey squares show the a^{14}C values of the stalagmite. (b) The according DCF [%] values for the different ^{14}C curves in (a) using the stalagmite a^{14}C values (lines are colour-coded).

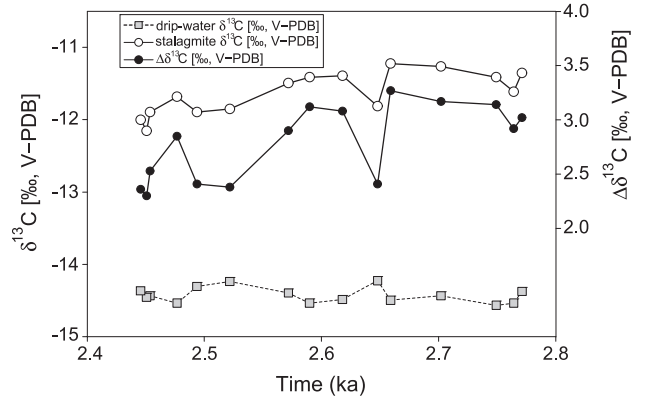

Fig. 6. (Left *y*-axis) Calculated initial drip water δ^{13}C (grey squares) compared with the 5-point running mean of the δ^{13}C from stalagmite LR06-B1 (white circles). (Right *y*-axis) The difference between the initial drip water δ^{13}C and the δ^{13}C of the calcite ($\Delta\delta^{13}$C, black circles) is due to fractionation effects in the cave, with higher values indicating more fractionation and lower values less fractionation. All data correspond to the depths and ages of the ^{14}C measurements.

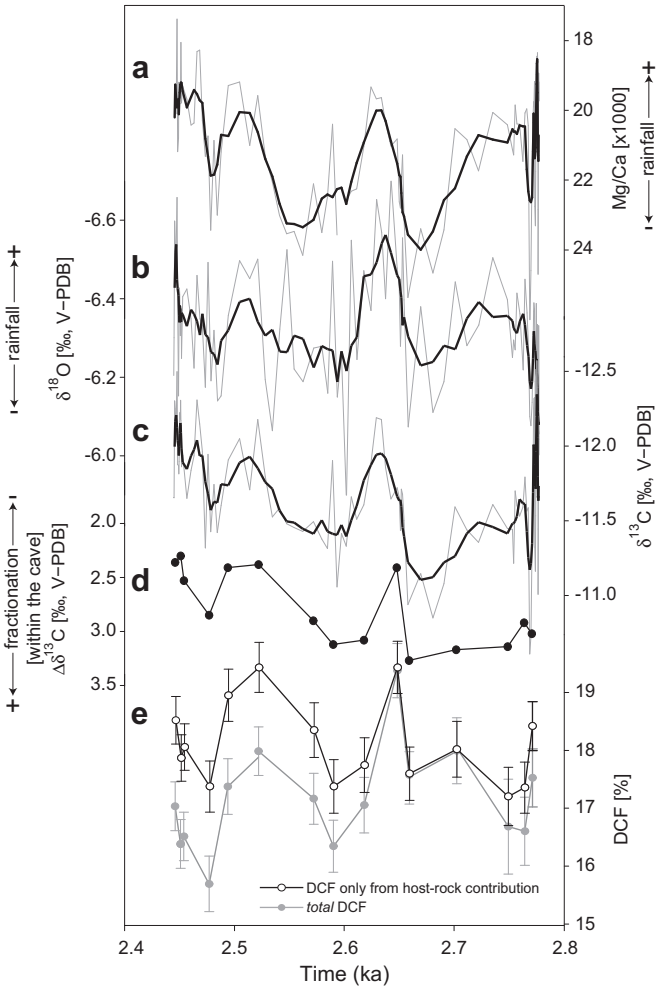

Fig. 7. Comparison of LR06-B1 (a) Mg/Ca ratios, (b) δ^{18}O, (c) δ^{13}C, (d) $\Delta\delta^{13}$C, and (e) DCF values (solid line: *total* DCF; dashed line: $DCF_{host\ rock}$).

open triangles). The next step is to separate the last two known influences: the host rock contribution and in-cave fractionation. Numerous cave-monitoring studies have demonstrated that fractionation in caves is kinetic rather than equilibrium in nature (Spötl et al., 2005; Frisia et al., 2011; Tremaine et al., 2011), thus precluding the use of equilibrium factors when estimating the fractionation effect. Therefore, we use the measured δ^{13}C of stalagmite LR06-B1 and initial δ^{13}C of soil-water DIC to further differentiate between host rock C contribution and fractionation effects inside the cave. To achieve this we must first estimate the soil-gas δ^{13}C, which we assume to be a typical −25‰ (Deines, 1980; Cerling, 1984), given that the soil above Liang Luar is dominated by C3 vegetation. Fractionation between gaseous CO_2 and HCO_3^- at 25 °C (~+7.9‰) increases the δ^{13}C of DIC in the soil-water to −17.1‰. Now that we can calculate the difference between the DIC and the stalagmite for both δ^{13}C and ^{14}C activity, it is possible to derive the extent of host rock contribution and fractionation in the cave with an iterative process using.

$\delta^{13}C = -2.4‰$ (measured value) and ^{14}C activity = 0 pMC for the host rock C isotopes as well as $^{14}\varepsilon$ (pMC) = 0.23 × $^{13}\varepsilon$ (‰) (Salièges and Fontes, 1984). For the computations, we use the 5-point running mean of the stalagmite δ^{13}C at each point of radiocarbon measurement.

Calculating the initial δ^{13}C of the calcite-saturated drip water is achieved by adding together the fraction of C originating from both

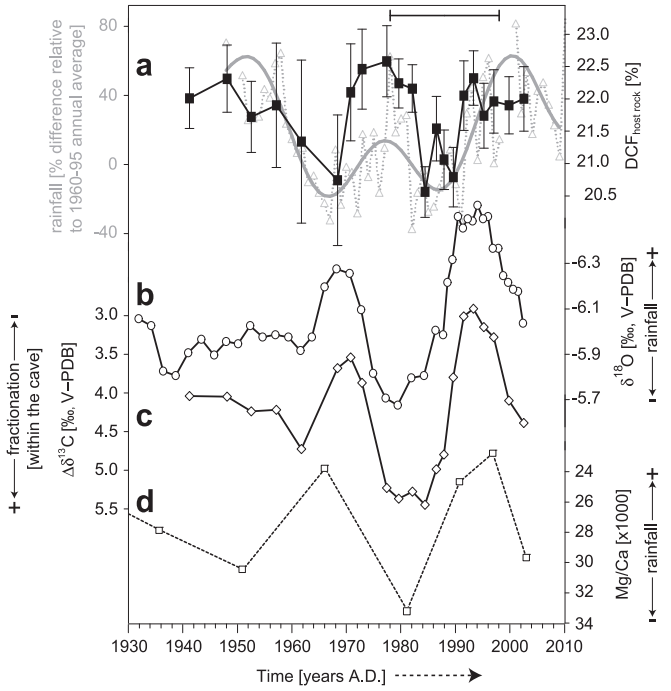

Fig. 8. Comparison between (a) $DCF_{host\ rock}$ and rainfall (NCEP/NCAR rainfall data at the nearest grid-point to Liang Luar and expressed as % difference relative to 1960–1995 average), (b) $\delta^{18}O$, (c) $\Delta\delta^{13}C$, and (d) Mg/Ca data for the instrumental period. All speleothem proxy data have been placed on the U-Th age model displayed in Fig. 2b. The 2σ (±10 years) error bar for the U-Th date used to construct the age model for the pre- and post-bomb period of the record is shown along the top.

the host rock ($\delta^{13}C = -2.4‰$) and DIC of the soil-water ($\delta^{13}C = -17.1‰$). For instance, if the stalagmite has a DCF vaue of 18% at time (t) and the corresponding ^{14}C activity of the initial DIC is 100 pMC (Fig. 5a), then the contribution of the host rock is 0.18, since the DIC is 100 pMC and the host rock is 0 pMC. Therefore, the $\delta^{13}C$ of the initial drip water at this point in time would equal:

$$\delta^{13}C_{drip\ \ water}(t) = [(0.18 \times -2.4‰) + (0.82 \times -17.1‰)] = -14.4‰$$

The difference between the above value and the corresponding calcite $\delta^{13}C$ value ($\Delta\delta^{13}C$) at t thus explains the fractionation in the cave (Figs. 6and 7d). For example, if the corresponding stalagmite $\delta^{13}C$ value at t equalled $-11.4‰$, then fractionation effects during calcite precipitation would explain the 3.0‰ offset between the two values. Given this, fractionation for ^{14}C would be ~6.9‰ or 0.69 pMC, which we then subtract from our measured stalagmite ^{14}C value at t.

We can then calculate the contribution of C from the host rock with:

$$DCF_{host\ \ rock} = [(1 - {}^{14}C_{initial\ drip-water}/{}^{14}C_{soil\ DIC}) \times 100]$$

Results of the $DCF_{host\ rock}$ calculations are presented in Fig. 5b (thin solid line with squares).

Because changes in fractionation in the cave (through ~2.4–2.8 ka interval) turn out to be rather small ($\Delta\delta^{13}C$ range = ~1‰ → ^{14}C range = ~0.23 pMC), relative to the much larger variations in DCF (Figs. 6and 7d), the $DCF_{host\ rock}$ profile (Fig. 5b, thin solid line with squares) lies almost parallel to the DCF curve that excludes $CO_2 \rightarrow HCO_3^-$ fractionation and vegetation effects (Fig. 5b, grey curve with open triangles). The most prominent feature of the $DCF_{host\ rock}$ profile is its strong resemblance with the *total* DCF curve, suggestive that variations in *total* DCF were indeed mostly due to changing inputs of host rock (modulated by changing open- versus closed-system conditions) to the karst water and hence the speleothem.

5.2. Hydrological control on speleothem DCF and $\delta^{13}C$

5.2.1. Late Holocene (~2.4–2.8 ka)

A striking feature of the late Holocene DCF profile of LR06-B1 (Fig. 7e) is its strong resemblance to the Mg/Ca (Fig. 7a), $\delta^{18}O$ (Fig. 7b), and $\delta^{13}C$ (Fig. 7c) series from the same stalagmite [previously reported in Griffiths et al. (2010a)]. Specifically, periods of lower Mg/Ca, $\delta^{18}O$, and $\delta^{13}C$ at ~2.77, 2.70, 2.64, 2.52, and 2.44 ka correspond with higher DCF values (Fig. 7e). Conversely, periods of higher Mg/Ca, $\delta^{18}O$, and $\delta^{13}C$ at ~2.66, 2.58, and 2.48 ka correspond with lower DCF values. The two largest DCF excursions at ~2.64 and ~2.52 ka, characterized by a ~2% increase in DCF, are matched by a 0.3–0.5‰ and 0.7–1.0‰ shift in $\delta^{18}O$ and $\delta^{13}C$ respectively. Previous work in Indonesia (e.g. Griffiths et al., 2009; Lewis et al., 2010) has demonstrated that the dominant process controlling the $\delta^{18}O$ of monsoon rainfall, and hence the speleothem calcite, is the 'amount effect' (Rozanski et al., 1992). This process, whereby lower (higher) $\delta^{18}O$ values correspond with higher (lower) rainfall, is underpinned by the strong co-variation with Mg/Ca (Fig. 7a), indicative of changes in the hydrology of the Liang Luar karst system (Griffiths et al., 2010a). The strong covariance between these different hydrologically-controlled proxies and DCF therefore suggests that the transport of radioactively dead carbon into Liang Luar is a function of rainfall above the cave. The question becomes: how did changes in hydrology affect the transport of dead carbon into the cave?

As demonstrated above, we infer the DCF signal in LR06-B1 to be primarily controlled by changes in the contribution of host rock C into the karst waters. It then follows that periods of higher (lower) cave recharge, inferred from lower (higher) Mg/Ca and $\delta^{18}O$ values, resulted in higher (lower) DCF values because the system may have been in a more closed (open) state. In other words, periods of low rainfall expose a larger number of air-filled voids in the epikarst because vadose dewatering exceeds vadose replenishment. This would facilitate gas exchange between the DIC of the karst water and soil atmosphere, which is characteristic of an open-system. Conversely, when rainfall is high, the voids in the soil and karst become filled, which would inhibit the potential of C isotope exchange between the DIC and soil-gas CO_2 (characteristic of a closed-system) and result in the proliferation of bedrock-derived dead carbon into the karst water. Physically, the effective diffusion rate of CO_2 determines the degree of open- to closed-system carbonate dissolution (Fohlmeister et al., 2011b). A similar relationship between rainfall amount and ^{14}C activity was detected in ^{14}C analyses of monthly collected cave drip waters from Grotta Di Ernesto, Italy (Fohlmeister et al., 2010). In addition, Oster et al. (2010) noted a positive relationship between rainfall amount and the ^{14}C activity of a deglacial-Holocene stalagmite from California. Although, contrary to our interpretation, these authors ruled out the host rock being the dominant influence on the DCF (based on $^{87}Sr/^{86}Sr$ ratios) and instead suggested that the turnover rate of the SOM was the more important influence.

Comparing the $\delta^{13}C$ profile (Fig. 7c) with the DCF record (Fig. 7e) reveals an anti-correlation between the two records (i.e. higher DCF values correspond with lower $\delta^{13}C$ and *vice versa*). This pattern is counterintuitive to what one would expect if the C isotopes of the DIC were in fact being driven by dissolution of the host rock. However, it is possible that such an increase in $\delta^{13}C$ (due to host rock contribution) may be more than offset by the effect of increased recharge on the rate of carbon dioxide degassing and

prior calcite precipitation (PCP). This possibility can be examined in more detail by comparing the $\delta^{13}C$ record (Fig. 7c) with the $\Delta\delta^{13}C$ profile (Fig. 7d), which is a proxy for in-cave fractionation. From Fig. 7, it is apparent that lower $\delta^{13}C$ values correspond with lower $\Delta\delta^{13}C$ values (or less fractionation), and *vice versa*. A similar pattern is observed when comparing the $\Delta\delta^{13}C$ with the Mg/Ca record (Fig. 7a). These phase relationships suggest that during wetter periods, when DCF values are high and Mg/Ca ratios are low, the C isotopes undergo less fractionation than would be the case during drier intervals when PCP is enhanced (Griffiths et al., 2010a). In general, wet periods permit less PCP (Fairchild et al., 2000; Fairchild and Treble, 2009) and tend to result in higher drip rates, which lead to less fractionation during stalagmite growth (Mühlinghaus et al., 2009; Scholz et al., 2009; Dreybrodt and Scholz, 2011) and hence higher stalagmite $\delta^{13}C$ values. Therefore, it is clear that for $\delta^{13}C$, variations in the host rock contribution are more than counterbalanced by variations in fractionation effects related to karst hydrology. These findings are consistent with our previous interpretation of the processes driving the $\delta^{13}C$ and Mg/Ca variability for the same Holocene stalagmite (Griffiths et al., 2010a).

As a final note, it is worth mentioning that whilst the *total* DCF and rainfall proxies show a similar structure, they also display slightly opposing trends (i.e. *total* DCF has a slight decreasing trend) through the 2.4–2.8 ka interval. However, the $DCF_{host\ rock}$ profile exhibits almost no trend or even a slight increasing trend, in agreement with the other rainfall proxies (Fig. 7e). The inversion of the trend is due to the influence of the vegetation. As discussed previously (see Section 5.1), fractionation between gaseous CO_2 and HCO_3^- is constant, and changes in the strength of fractionation between HCO_3^- of the calcite-saturated solution and the precipitated $CaCO_3$, has little influence on the $Ca^{14}CO_3$ (as described in Section 5.1.2). Hence, the opposing trends between the *total* DCF and the $DCF_{host\ rock}$ can be ascribed to the smoothing characteristics of the vegetation, as evident in comparing the atmospheric ^{14}C (dashed line) and the soil-gas CO_2 (black solid line; represents an integrated mixture of past atmospheric ^{14}C levels) profiles in Fig. 5a.

5.2.2. Instrumental period

As recognised earlier, the ^{14}C measurements through the bomb pulse scatter around the fitted curve (Fig. 4). The interpretation of DCF variability during the late Holocene (2.4–2.8 ka) could lead one to conclude that the host rock contribution was not constant during the pre- and post-bomb period, but varied in response to hydrological changes over the past 70 years (Fig. 8). On the one hand, fluctuations in DCF can make the estimation of the SOM age spectrum somewhat more difficult because the scattered values increase the uncertainty of the fit. However, on the other hand, a non-constant C entry from the host-rock presents us with the opportunity of testing whether the precipitation dependence of the DCF was also observed during the instrumental era. Hence, it allows us to establish whether or not our late Holocene hypothesis is robust. Therefore, we now adapt the analysis procedure performed in Section 5.1.1 to the ^{14}C data through the bomb pulse. We retain the same SOM age spectrum, but now reanalyse the bomb ^{14}C data according to the method described in Section 5.1.2.

From Fig. 8, it is clear that there were significant variations in $DCF_{host\ rock}$ during the pre- and post-bomb intervals in response to changes in local rainfall (Fig. 8a). Indeed, two prominent rainfall phases (characterized by an increase of 30–40%) centred around 1975 and 1995, were matched [within analytical uncertainty (±10 years) of the U-Th age model] by a ~1.5% increase in $DCF_{host\ rock}$ (Fig. 8a). These perturbations are echoed in the proxy data, which display a ~0.5–0.8‰ decrease in $\delta^{18}O$ (Fig. 8b), a ~2–3‰ decrease in $\Delta\delta^{13}C$ (less fractionation; Fig. 8c), and an increase in Mg/Ca (less PCP; Fig. 8d); while only seven Mg/Ca data points are shown in Fig. 8c, a strong relationship between this proxy and the stable-isotopes (of the same specimen) was observed for the entire Holocene (see Griffiths et al., 2010a). Hence, this result supports our conclusion that the DCF activity in our speleothem was dominated by fluctuating Liang Luar karst hydrology.

An equally, if not more, important finding, is the responsiveness of the DCF to rapid changes in rainfall observed throughout the mid to late 20th century. This result is quite compelling as it highlights the sensitivity of the DCF to abrupt shifts in local hydrology. Moreover, comparing the scale of the shifts in both DCF and rainfall over this period, reveals that a relatively modest change in precipitation (~30%), as compared with the changes observed through the Holocene (Griffiths et al., 2009), can result in relatively large shifts in the DCF (>1.5%). This observation, therefore, casts doubt on the stable nature of the DCF in LR06-B1 over much longer time scales, when boundary conditions were certainly different from today (e.g. Last Glacial Maximum). Whether this pattern is purely a local signal (in terms of both the speleothem and/or cave), or more regionally-synchronous in nature, is yet to be confirmed. This emphasises the need for more research on the DCF behaviour of tropical speleothems over longer time scales and during known climate events (e.g. Younger Dryas), especially in light of the renewed interest in using these deposits to extend the radiocarbon calibration curve (e.g. Hoffmann et al., 2010).

6. Conclusions

In this study, we have assessed the dead carbon content of the late Holocene section of speleothem LR06-B1, which was recovered from the island of Flores, Indonesia. DCF values were established using coupled AMS ^{14}C measurements and U-Th dating through an interval of the late Holocene (~2.4–2.8 ka) marked by a prominent excursion in atmospheric radiocarbon content. In addition, ^{14}C measurements through the pre- and post-bomb periods (~1940–2000 A.D.) provided the input parameters to a soil-host rock-cave model (Genty and Massault, 1999; Fohlmeister et al., 2011a), which was used to explore soil-karst C dynamics above and within Liang Luar. By coupling the stalagmite ^{14}C measurements with the C model output, we were able to separate each of the known C reservoirs contributing to the *total* DCF content of the speleothem. In doing so, we found that the DCF was predominantly controlled by dissolution of the host limestone (associated with changes in open- and closed-system conditions) rather than kinetic fractionation and/or variations in the age spectrum of the SOM.

The *corrected* DCF curve (i.e. corrected for vegetation/SOM and fractionation effects, and hence contains only the contribution from the host-rock), was then compared with stable-isotope ($\delta^{13}C$ and $\delta^{18}O$) and trace-element (Mg/Ca) data from the same specimen [previously reported in Griffiths et al. (2009, 2010a)]. We found that over the 2.4–2.8 ka interval, periods of lower (higher) Mg/Ca, $\delta^{18}O$, and $\delta^{13}C$ values, indicative of wetter (drier) conditions, corresponded with higher (lower) DCF values. This higher DCF input during periods of higher cave recharge was interpreted to reflect more closed-system conditions, when the water-filled voids in the soil and epikarst inhibited the potential of C isotope exchange between the DIC and soil-gas CO_2. In contrast, lower DCF input was interpreted to reflect more open-system conditions, when periods of lower rainfall exposed a larger number of air-filled voids in the epikarst and thus facilitated gas exchange between the DIC of the karst water and soil atmosphere. These patterns were strongly supported by the comparison of pre- and post-bomb DCF values with instrumental rainfall records (during the mid to late 20th century), which, similar to the late Holocene, highlight that DCF was controlled by local hydrology. This strong DCF-rainfall link

therefore suggests that the DCF in our speleothem provides us with an additional climate proxy with which to reconstruct past changes in monsoon rainfall.

Some studies have demonstrated that speleothems may provide a potential utility for the improvement/extension of the widely-used radiocarbon timescale (e.g. Beck et al., 2001; Hoffmann et al., 2010). However, the observed link between DCF and local hydrology in the Liang Luar soil-karst system stresses the need for more detailed research (including both additional measurements and modelling) on the transport of ^{14}C, and hence DCF, within soil-host rock-cave systems. In addition, our findings highlight that stable- and radiogenic-C-isotope data can be used to unravel the different processes governing the isotope variability of karst waters prior to speleothem growth. Together with other climate proxies such as $\delta^{18}O$ and/or Mg/Ca ratios, these results show that it is possible to gain a clearer picture of the soil-to-cave carbon transfer dynamics through time, including a detailed appraisal of the possible causes and effects. Therefore, for studies aimed at reconstructing past atmospheric ^{14}C concentrations from speleothems, we strongly recommend that researchers present not only precise ^{14}C and absolute ages but also additional proxy information useful for constraining temporal DCF variability.

Finally, we have demonstrated that it is possible to estimate the initial $\delta^{13}C$ of DIC in the drip water using the combined stalagmite ^{14}C and $\delta^{13}C$ measurements. Estimating this value is very important for modelling studies aiming to describe isotope fractionation effects during calcite precipitation (Scholz et al., 2009; Mühlinghaus et al., 2009; Dreybrodt and Scholz, 2011). Also, by calculating the difference between initial drip water $\delta^{13}C$ and calcite $\delta^{13}C$, it is possible to derive quantitative estimations of the drip interval, which would be especially beneficial for stalagmite samples/studies that did not experience PCP.

Acknowledgements

The authors wish to thank W.S. Hantoro, B. Suwargadi, N. Anderson, G. Smith, J. Rutledge, S. Lewis, E. St Pierre, E. Yulianto, and the Indonesian Institute of Sciences (LIPI) for logistical support and technical assistance with fieldwork, which was carried out under LIPI Research Permit number 2748/SU.3/KS/2007. We also thank members of the AMS team at the Australian Nuclear Science and Technology Organisation (ANSTO) for their help with sample preparation and AMS measurements. This research was supported by the NOAA/UCAR Climate and Global Change Postdoctoral Fellowship to M.L.G., an Australian Institute of Nuclear Science and Engineering (AINSE) award for AMS ^{14}C analyses (Grants 08/146 and 10/148) to R.N.D. and M.L.G., and an Australian Research Council *Discovery* grant DP0663274 to M.K.G., R.N.D., and W.S.H. J.F. was funded by the German Science Foundation (research group 668 – Daphne). This study was greatly improved through helpful comments and suggestions from Christoph Spötl, Dirk Hoffmann and an anonymous reviewer.

*Editorial handling by:*C. Spotl

References

Abram, N.J., McGregor, H.V., Gagan, M.K., Hantoro, W.S., Suwargadi, B.W., 2009. Oscillations in the southern extent of the Indo-Pacific warm pool during the mid-Holocene. Quaternary Science Reviews 28, 2794–2803.

Anshari, G., Kershaw, A.P., van der Kaars, S., 2001. A late Pleistocene and Holocene pollen and charcoal record from peat swamp forest, Lake Sentarum Wildlife Reserve, west Kalimantan, Indonesia. Palaeogeography, Palaeoclimatology, Palaeoecology 171, 213–228.

Beck, J.W., Richards, D.A., Edwards, R.L., Silverman, B.W., Smart, P.L., Donahue, D.J., Hererra-Osterheld, S., Burr, G.S., Calsoyas, L., Jull, A.J.T., Biddulph, D., 2001. Extremely large variations of atmospheric C-14 concentration during the last glacial period. Science 292, 2453–2458.

Blyth, A.J., Baker, A., Thomas, L.E., Van Calsteren, P., 2011. A 2000-year lipid biomarker record preserved in a stalagmite from north-west Scotland. Journal of Quaternary Science 26, 326–334.

Broecker, W.S., Olson, E.A., Orr, P.C., 1960. Radiocarbon measurements and annual rings in cave formations. Nature 185, 93–94.

Cerling, T.E., 1984. The stable isotopic composition of modern soil carbonate and its relationship to climate. Earth and Planetary Science Letters 71, 229–240.

Cheng, H., Edwards, R.L., Hoff, J., Gallup, C.D., Richards, D.A., Asmerom, Y., 2000. The half-lives of uranium-234 and thorium-230. Chemical Geology 169, 17–33.

Deines, P., 1980. The Isotopic Composition of Reduced Organic Soil. Elsevier, Amsterdam, Oxford, New York, Tokyo. 329–406.

Dorale, J.A., Onac, B.P., Fornos, J.J., Gines, J., Gines, A., Tuccimei, P., Peate, D.W., 2010. Sea-level highstand 81,000 years ago in mallorca. Science 327, 860–863.

Dörr, H., Münnich, K.O., 1986. Annual variations of the C-14 content of soil CO_2. Radiocarbon 28, 338–345.

Dreybrodt, W., Scholz, D., 2011. Climatic dependence of stable carbon and oxygen isotope signals recorded in speleothems: from soil water to speleothem calcite. Geochimica et Cosmochimica Acta 75, 734–752.

Drysdale, R.N., Hellstrom, J.C., Zanchetta, G., Fallick, A.E., Goni, M.F.S., Couchoud, I., McDonald, J., Maas, R., Lohmann, G., Isola, I., 2009. Evidence for obliquity forcing of glacial termination II. Science 325, 1527–1531.

Drysdale, R.N., Zanchetta, G., Hellstrom, J.C., Fallick, A.E., McDonald, J., Cartwright, I., 2007. Stalagmite evidence for the precise timing of north Atlantic cold events during the early last glacial. Geology 35, 77–80.

Drysdale, R.N., Zanchetta, G., Hellstrom, J.C., Fallick, A.E., Zhao, J.X., 2005. Stalagmite evidence for the onset of the Last Interglacial in southern Europe at 129 +/−1 ka. Geophysical Research Letters 32, L24708. doi:10.1029/2005GL024658.

Dublyansky, Y.V., Spötl, C., 2009. Hydrogen and oxygen isotopes of water from inclusions in minerals: design of a new crushing system and on-line continuous-flow isotope ratio mass spectrometric analysis. Rapid Communications in Mass Spectrometry 23, 2605–2613.

Fairchild, I.J., Borsato, A., Tooth, A.F., Frisia, S., Hawkesworth, C.J., Huang, Y.M., McDermott, F., Spiro, B., 2000. Controls on trace element (Sr-Mg) compositions of carbonate cave waters: implications for speleothem climatic records. Chemical Geology 166, 255–269.

Fairchild, I.J., Treble, P., 2009. Trace elements in speleothems as recorders of environmental change. Quaternary Science Reviews 28, 449–468.

Fink, D., Hotchkis, M., Hua, Q., Jacobson, G., Smith, A.M., Zoppi, U., Child, D., Misfud, C., van der Gaast, H., Williams, A., Williams, M., 2004. The ANTARES AMS facility at ANSTO. Nuclear Instruments and Methods in Physics Research B 223–224, 109–115.

Fohlmeister, J., Kromer, B., Mangini, A., 2011a. The influence of soil organic matter age spectrum on the reconstruction of atmospheric ^{14}c levels via stalagmites. Radiocarbon 53, 99–115.

Fohlmeister, J., Scholz, D., Kromer, B., Mangini, A., 2011b. Modelling carbon isotopes of carbonates in cave drip water. Geochimica et Cosmochimica Acta 238, 239–245.

Fohlmeister, J., Schröder-Ritzrau, A., Spötl, C., Frisia, S., Miorandi, R., Kromer, B., Mangini, A., 2010. The influences of hydrology on the radiogenic and stable carbon isotope composition of cave drip water, Grotta Di Ernesto (Italy). Radiocarbon 52, 1529–1544.

Frisia, S., Fairchild, I.J., Fohlmeister, J., Miorandi, R., Spötl, C., Borsato, A., 2011. Carbon mass-balance modelling and carbon isotope exchange processes in dynamic caves. Geochimica et Cosmochimica Acta 75, 380–400.

Genty, D., Baker, A., Massault, M., Proctor, C., Gilmour, M., Pons-Branchu, E., Hamelin, B., 2001. Dead carbon in stalagmites: carbonate bedrock paleodissolution vs. ageing of soil organic matter. Implications for ^{13}C variations in speleothems. Geochimica et Cosmochimica Acta 65, 3443–3457.

Genty, D., Massault, M., 1999. Carbon transfer dynamics from bomb-C-14 and delta C-13 time series of a laminated stalagmite from SW France – Modelling and comparison with other stalagmite records. Geochimica et Cosmochimica Acta 63, 1537–1548.

Genty, D., Massault, M., Gilmour, M., Baker, A., Verheyden, S., Kepens, E., 1999. Calculation of past dead carbon proportion and variability by the comparison of AMS ^{14}C and TIMS U/Th ages on two Holocene stalagmites. Radiocarbon 41, 251–270.

Griffiths, M.L., Drysdale, R.N., Gagan, M.K., Frisia, S., Zhao, J.X., Ayliffe, L.K., Hantoro, W.S., Hellstrom, J.C., Fischer, M.J., Feng, Y.X., Suwargadi, B.W., 2010a. Evidence for Holocene changes in Australian-Indonesian monsoon rainfall from stalagmite trace element and stable isotope ratios. Earth and Planetary Science Letters 292, 27–38.

Griffiths, M.L., Drysdale, R.N., Gagan, M.K., Zhao, J.X., Ayliffe, L.K., Hellstrom, J.C., Hantoro, W.S., Frisia, S., Feng, Y.X., Cartwright, I., Pierre, E.S., Fischer, M.J., Suwargadi, B.W., 2009. Increasing Australian-Indonesian monsoon rainfall linked to early Holocene sea-level rise. Nature Geoscience 2, 636–639.

Griffiths, M.L., Drysdale, R.N., Vonhof, H.B., Gagan, M.K., Zhao, J.X., Ayliffe, L.K., Hantoro, W.S., Hellstrom, J.C., Cartwright, I., Frisia, S., Suwargadi, B.W., 2010b. Younger Dryas-Holocene temperature and rainfall history of southern Indonesia from $\delta^{18}O$ in speleothem calcite and fluid inclusions. Earth and Planetary Science Letters 295, 30–36.

Hellstrom, J., 2003. Rapid and accurate U/Th dating using parallel ion-counting multi-collector ICP-MS. Journal of Analytical Atomic Spectrometry 18, 1346–1351.

Hellstrom, J.C., 2006. U–Th dating of speleothems with high initial ^{230}Th using stratigraphical constraint. Quaternary Geochronology 1, 289–295.

Hendy, C.H., 1971. The isotopic geochemistry of speleothems: the calculations of the effects of different modes of Formation on the isotopic composition of speleothems and their applicability as palaeoclimate indicators. Geochimica et Cosmochimica Acta 35, 801–824.

Hendy, C.H., Wilson, A.T., 1968. Palaeoclimatic data from speleothems. Nature 219, 48–51.

Hodge, E., McDonald, J., Fischer, M., Redwood, D., Hua, Q., Levchenko, V., Drysdale, R., Waring, C., Fink, D., 2011. Using the ^{14}C bomb pulse to date young speleothems. Radiocarbon 53, 345–357.

Hoffmann, D.L., Beck, J.W., Richards, D.A., Smart, P.L., Singarayer, J.S., Ketchmark, T., Hawkesworth, C.J., 2010. Towards radiocarbon calibration beyond 28 ka using speleothems from the Bahamas. Earth and Planetary Science Letters 289, 1–10.

Hope, G., 2001. Environmental change in the late Pleistocene and later Holocene at Wanda site, Soroako, South Sulawesi, Indonesia. Palaeogeography, Palaeoclimatology, Palaeoecology 171, 129–145.

Hua, Q., Barbetti, M., 2004. Review of tropospheric bomb ^{14}C data for carbon cycle modeling and age calibration purposes. Radiocarbon 46, 1273–1298.

Hua, Q., Barbetti, M., Jacobsen, G.E., Zoppi, U., Lawson, E.M., 2000. Bomb radiocarbon in annual tree rings from Thailand and Australia. Nuclear Instruments and Methods in Physics Research B 172, 359–365.

Hua, Q., Jacobsen, G.E., Zoppi, U., Lawson, E.M., Williams, A.A., Smith, A.M., McGann, M.J., 2001. Progress in radiocarbon target preparation at the ANTARES AMS Centre. Radiocarbon 43, 275–282.

Hua, Q., Barbetti, M., Zoppi, U., Chapman, D.M., Thomson, B., 2003. Bomb radiocarbon in tree rings from northern New South Wales, Australia: implications for dendrochronology, atmospheric transport, and air-sea exchange of CO_2. Radiocarbon 45, 431–447.

Kluge, T., Marx, T., Scholz, D., Niggemann, S., Mangini, A., Aeschbach-Hertig, W., 2008. A new tool for palaeoclimate reconstruction: noble gas temperatures from fluid inclusions in speleothems. Earth and Planetary Science Letters 269, 407–414.

Lewis, S.C., LeGrande, A.N., Kelley, M., Schmidt, G.A., 2010. Water vapour source impacts on oxygen isotope variability in tropical precipitation during Heinrich events. Climate of the Past 6, 325–343.

McCormac, F.G., Hogg, A.G., Blackwell, P.G., Buck, C.E., Higham, T.F.G., Reimer, P.J., 2004. SHCal04 Southern Hemisphere calibration, 0–11.0 cal kyr BP. Radiocarbon 46, 1087–1092.

Monk, K.A., De Fretes, V., Reksodiharjo-Lilley, G., 1997. The Ecology of Nusa Tenggara and Maluku. In: The Ecology of Indonesia Series, vol. 5. Periplus Editions (HK) Ltd, Singapore.

Mook, W.G., de Vries, J.J., 2000. Environmental Isotopes in the Hydrological Cycle Principles and Applications – Volume I: Introduction – Theory, Methods, Review. IAEA, Vienna.

Mühlinghaus, C., Scholz, D., Mangini, A., 2009. Modeling fractionation of stable isotopes in stalagmites. Geochimica et Cosmochimica Acta 71, 2780–2790.

Oster, J.L., Montanez, I.P., Guilderson, T.P., Sharp, W.D., Banner, J.L., 2010. Modeling speleothem $\delta^{13}C$ variability in a central Sierra Nevada cave using ^{14}C and $^{87}Sr/^{86}Sr$. Geochimica et Cosmochimica Acta 74, 5228–5242.

Reimer, P.J., Baillie, M.G.L., Bard, E., Bayliss, A., Beck, J.W., Bertrand, C.J.H., Blackwell, P.G., Buck, C.E., Burr, G.S., Cutler, K.B., Damon, P.E., Edwards, R.L., Fairbanks, R.G., Friedrich, M., Guilderson, T.P., Hogg, A.G., Hughen, K.A., Kromer, B., McCormac, G., Manning, S., Ramsey, C.B., Reimer, R.W., Remmele, S., Southon, J.R., Stuiver, M., Talamo, S., Taylor, F.W., van der Plicht, J., Weyhenmeyer, C.E., 2004. IntCal04 terrestrial radiocarbon age calibration, 0–26 cal kyr BP. Radiocarbon 46, 1029–1058.

Reimer, P.J., Baillie, M.G.L., Bard, E., Bayliss, A., Beck, J.W., Blackwell, P.G., Ramsey, C.B., Buck, C.E., Burr, G.S., Edwards, R.L., Friedrich, M., Grootes, P.M., Guilderson, T.P., Hajdas, I., Heaton, T.J., Hogg, A.G., Hughen, K.A., Kaiser, K.F., Kromer, B., McCormac, F.G., Manning, S.W., Reimer, R.W., Richards, D.A., Southon, J.R., Talamo, S., Turney, C.S.M., van der Plicht, J., Weyhenmeye, C.E., 2009. Intcal09 and marine09 radiocarbon age calibration curves, 0–50,000 Years Cal Bp. Radiocarbon 51, 1111–1150.

Rozanski, K., Araguasaraguas, L., Gonfiantini, R., 1992. Relation between long-term trends of O-18 isotope composition of precipitation and climate. Science 258, 981–985.

Rudzka, D., McDermott, F., Baldini, L.M., Fleitmann, D., Moreno, A., Stoll, H., 2011. The coupled $\delta^{13}C$ -radiocarbon systematics of three Late Glacial/early Holocene speleothems; insights into soil and cave processes at climatic transitions. Geochimica et Cosmochimica Acta 75, 4321–4339.

Salièges, J.F., Fontes, J.C., 1984. Essai de Détermination Expérimentale du Fractionnement des Isotopes ^{13}C et ^{14}C du Carbone au cours de Processus Naturels. International Journal of Applied Radiation and Isotopes 35, 55–62.

Scholz, D., Mühlinghaus, C., Mangini, A., 2009. Modelling $\delta^{13}C$ and $\delta^{18}O$ in the solution layer on stalagmite surfaces. Geochimica et Cosmochimica Acta 73, 2592–2602.

Southon, J.R., Noronha, A.L., Cheng, H., Edwards, R.L., Wang, Y., 2012. A high-resolution record of atmospheric ^{14}C based on Hulu cave speleothem H82. Quaternary Science Reviews 33, 32–41.

Spötl, C., Fairchild, I.J., Tooth, A.F., 2005. Cave air control on dripwater geochemistry, Obir Caves (Austria): implications for speleothem deposition in dynamically ventilated caves. Geochimica et Cosmochimica Acta 69, 2451–2468.

Stott, L., Cannariato, K., Thunell, R., Haug, G.H., Koutavas, A., Lund, S., 2004. Decline of surface temperature and salinity in the western tropical Pacific Ocean in the Holocene epoch. Nature 431, 56–59.

Tremaine, D.M., Froelich, P.N., Wang, Y., 2011. Speleothem calcite farmed in situ: modern calibration of $\delta^{18}O$ and $\delta^{13}C$ paleoclimate proxies in a continuously-monitored natural cave system. Geochimica et Cosmochimica Acta 75, 4929–4950.

Trumbore, S., 2000. Age of soil organic matter and soil respiration: radiocarbon constraints on belowground C dynamics. Ecological Applications 10, 399–411.

van Bemmelen, R.W., 1949. The Geology of Indonesia. In: General Geology of Indonesia and Adjacent Archipelagos, vol. 1. A. Government Printing Office, The Hague.

Van Der Kaars, S., Penny, D., Tibby, J., Fluin, J., Dam, R., Suparan, P., 2001. Late Quaternary palaeoecology, palynology and palaeolimnology of a tropical lowland swamp: Rawa Danau, West-Java, Indonesia. Palaeogeography, Palaeoclimatology, Palaeoecology 171, 185–212.

Vonhof, H.B., van Breukelen, M.R., Postma, O., Rowe, P.J., Atkinson, T.C., Kroon, D., 2006. A continuous-flow crushing device for on-line $\delta^{2}H$ analysis of fluid inclusion water in speleothems. Rapid Communications in Mass Spectrometry 20, 2553–2558.

Wackerbarth, A., Scholz, D., Fohlmeister, J., Mangini, A., 2010. Modelling the $\delta^{18}O$ value of cave drip water and speleothem calcite. Earth and Planetary Science Letters 299, 387–397.

Wang, Y.J., Cheng, H., Edwards, R.L., Kong, X.G., Shao, X.H., Chen, S.T., Wu, J.Y., Jiang, X.Y., Wang, X.F., An, Z.S., 2008. Millennial- and orbital-scale changes in the East Asian monsoon over the past 224,000 years. Nature 451, 1090–1093.

Westaway, K.E., 2006. Reconstructing the Quaternary landscape evolution and climate history of western Flores: an environmental and chronological context for an archaeological site. Ph.D. Dissertation, University of Wollongong, Australia.

Woodhead, J., Hellstrom, J., Maas, R., Drysdale, R., Zanchetta, G., Devine, P., Taylor, E., 2006. U-Pb geochronology of speleothems by MC-ICPMS. Quaternary Geochronology 1, 208–221.

Yu, K.F., Zhao, J.X., Shi, Q., Chen, T.G., Wang, P.X., Collerson, K.D., Liu, T.S., 2006. U-series dating of dead Porites corals in the South China sea: evidence for episodic coral mortality over the past two centuries. Quaternary Geochronology 1, 129–141.

Zhao, J.X., Xia, Q.K., Collerson, K.D., 2001. Timing and duration of the Last Interglacial inferred from high resolution U-series chronology of stalagmite growth in Southern Hemisphere. Earth and Planetary Science Letters 184, 635–644.

Zhou, H., Zhao, J.X., Qing, W., Feng, Y., Tang, J., 2011. Speleothem-derived Asian summer monsoon variations in Central China, 54–46 ka. Journal of Quaternary Science. doi:10.1002/jqs.1506.